EFFECT OF ELECTRIC FIELDS ON THE SYNTHESIS OF NANOPARTICLES OF TIN AND SILICON IN A LIQUID ENVIRONMENT

A THESIS IN
PHYSICS

Presented to the Faculty of the University
of Missouri-Kansas City in partial fulfillment of
the requirements for the degree

MASTER OF SCIENCE

by
DEEPAK SAPKOTA
M.Sc., Tribhuvan University, 2006

Kansas City, Missouri
2015

EFFECT OF ELECTRIC FIELDS ON THE SYNTHESIS OF NANOPARTICLES OF TIN AND SILICON IN A LIQUID ENVIRONMENT

Deepak Sapkota, Candidate for the Master of Science Degree

University of Missouri-Kansas City, 2015

ABSTRACT

The effect of externally applied electric fields on the size and morphology of nanoparticles fabricated by laser ablation was investigated. In this method, a pulsed laser beam was focused onto a solid target of either silicon or tin and the laser beam ablated the target at the liquid-solid interface. The laser beam vaporizes the target material forming a plasma plume which contains ions, electrons, nanoparticles, and nano clusters. High pressures, high temperatures and high energy densities are created in this method. These conditions are favorable for the formation of metastable phases resulting in novel products depending on the nature of the liquid and solid. The ablated products were studied under bright field transmission electron microscopy and high resolution transmission electron microscopy. It has been found that the sizes of the nanoparticles were influenced by the application of an externally applied electric field during laser irradiation.

Key words: Silicon, tin, pulsed laser ablation, nanoparticles, morphology

APPROVAL

The faculty listed below, appointed by the Dean of the College of Arts and Sciences have examined a thesis titled "Effect of Electric Fields on the Synthesis of Nanoparticles in a Liquid Environment," presented by Deepak Sapkota, candidate for the Master of Science degree, and certify that in their opinion it is worthy of acceptance.

Supervisory Committee

Michael Kruger, Ph.D., Committee Chair

Department of Physics and Astronomy

Jerzy M. Wrobel, Ph.D.

Department of Physics and Astronomy

Da-Ming Zhu, Ph.D.

Department of Physics and Astronomy

TABLE OF CONTENTS

Page

LIST OF ILLUSTRATIONS

Figure Page

LIST OF TABLES

ACKNOWLEDGEMENTS

I would like to sincerely thank my academic advisor Professor Michael Kruger for his guidance, support and advice in accomplishing my research thesis. I am very lucky to have him as my advisor.

I would like to convey my sincere gratitude to Dr. Omar Musaev and Mr. Yilu Li for their contributions to my thesis. I would also like to thank Professor Jerzy Wrobel for his cooperation and suggestion in completing my research work in time. I am grateful to all friends who directly or indirectly helped me by offering their valuable advice and comments towards improving my research work. I am also very thankful to the Department of Physics and Astronomy, UMKC, for providing financial aid in the form of a teaching assistantship.

Finally and most importantly, I would like to thank with lots of love to my wife Seema Adhikari Sapkota for her understanding, support and encouragement throughout my work.

Dedicated to my wife Seema Adhikari Sapkota and our parents

CHAPTER 1

INTRODUCTION

1.1 Laser:

LASER[1] is an acronym for Light Amplification by Stimulated Emission of Radiation. The advent of the laser[2] has created new fields in the scientific world. Laser light is monochromatic, coherent, collimated and unidirectional.[3] Other remarkable features of laser light are its high energy density and low divergence. Due to the unique properties of laser light, lasers are important devices used in various applications.

Today, lasers can be found in a broad range of applications throughout the world in industry and research fields like physics, chemistry, biology and medicine. They are widely used in welding[4], cutting[5], printing[6,7] and communication[8]. Recently, lasers have been used in the ablation of solids and liquids for the formation of novel nanocrystals and the fabrication of nanostructures.

1.2 History of laser:

The working of the laser is based on the principle of stimulated emission proposed by Albert Einstein in 1917.[9] The theory of stimulated emission was first realized practically in the MASER (Microwave Amplification by Stimulated Emission of Radiation). The physics behind the operation of the maser was first described by Dr. Nikolay Basov and Dr. Alexander Prochorov at the Lebedev Institute of Physics in Moscow in 1954.[10,11] Simultaneously and independently, Charles Townes and his coworkers at Columbia University in New York built the first maser in 1953.[12] They applied the idea of stimulated

emission to excited ammonia molecules to produce amplified microwaves. They produced uniform radiation of a single wavelength in the microwave region. The power was very tiny (~ 10 nW). Basov, Prochorov and Townes received the Nobel Prize[13] in 1964 for their contributions to physics.

With the success of the maser, researchers started studying how to extend the maser concept to the infrared and visible regions. Gordon Gould was credited for creating the acronym LASER. In fact, he had been interested in a project to build an optical maser which he renamed laser. The first working laser was built by Theodore Maiman at Hughes Research Lab in California in 1960.[14] The laser he built used a cylindrical ruby crystal and emitted light with a wavelength of 694 nm. The first gas laser was He-Ne laser that produced a laser beam in the infrared region of the spectrum. The first excimer gas laser[15] based only on xenon was constructed by Nikaloi Basov, VA Danilychev and Yu.M. Popov at the Lebedev Institute of Physics in Moscow in 1970.

1.3 Principle of laser operation:

The laser works on the principle of stimulated emission. Stimulated emission is a process in which incoming photons interact with electrons that are in an excited atomic level, with the resulting emission of new photons which have the same phase, frequency and direction as the incident photons. When an electron moves from one energy level to another energy level, emission or absorption of energy occurs which is equal to the energy difference between the two levels. This is governed by the quantization of energy levels postulated by Niels Bohr.[16]

$$E_{photon} = h\nu = E_{n_2} - E_{n_1} \quad (1.1)$$

where E_{n_2} and E_{n_1} are the higher and lower energy levels respectively.

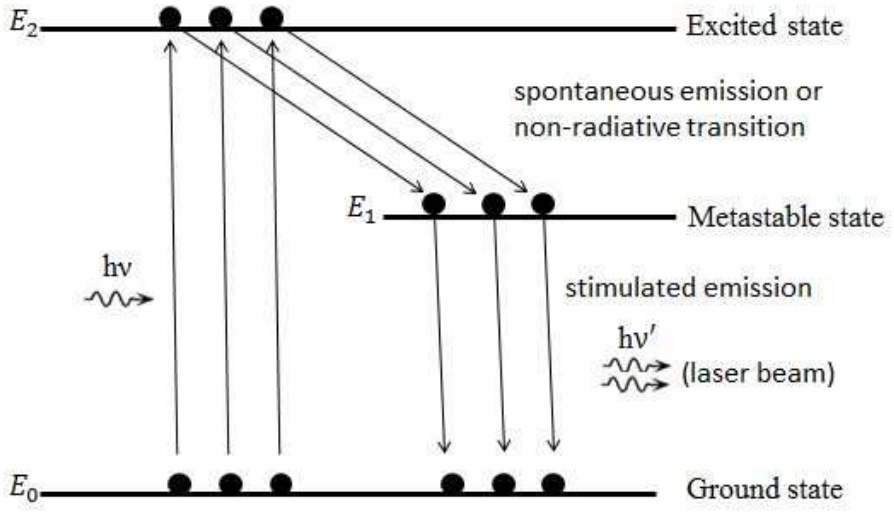

Figure 1.1: Three energy level diagram depicting stimulated emission.

To initiate the process of stimulated emission, there should be a large number of atoms in an excited level, which is referred to as population inversion. If a population inversion exists, stimulated emission can produce significant light amplification. One method to achieve a population inversion is through optical pumping. Optical pumping is a method in which energy is transferred, by means of electromagnetic radiation, from an external source to electrons in a lower energy level to excite them into a higher energy level. The lifetime of an electron in the excited state is very short (~ 10^{-8} sec). It may undergo spontaneous emission or non-radiative transition to a metastable state or ground state. Long-lived excited states are often called metastable states (life time~ 10^{-5} sec). Once a population inversion is achieved, electrons in the metastable state are induced to jump to the ground state by the presence of

photons as shown in figure 1.1. The result is photons with the same energy travelling in the same direction. The repetition of this produces a laser beam.

1.4 Laser ablation:

Laser ablation[17] is the process of removing material from a solid surface by irradiating it with a laser beam. When a low fluence laser beam is incident on a solid surface, it interacts with the material and some of the light is transformed into heat, leading to an increase in the temperature of the solid. For a sufficiently intense laser beam, the surface sublimates or melts and evaporates. With a high fluence laser, the temperature of the solid surface becomes high (5000 K or higher) very quickly and the surface undergoes a rapid transition, from superheated liquid to a mixture of vapor and liquid droplets. This causes the formation of plasma which may contain free electrons, ions and solid particles with nano dimensions.

Laser ablation has widespread applications in research and industry[18]. Laser ablation technology is used in surgery[19], drilling[20,21], cutting[5], and other fields. In 1965, Smith and Turner used pulsed laser deposition for the preparation of semiconductor and dielectric thin films[22]. In recent decades, it has been used in the preparation of thin films[23], formation of novel nano crystals[24] and the fabrication of nano structures. In 1995, Richard Smalley and co-workers at Rice University used pulsed laser ablation to irradiate a graphite target at high temperature and produced carbon nano tubes[25]. It has become a very promising method in nanotechnology research.[26]

1.4.1 Laser ablation of a solid in a gaseous environment:

Pulsed laser ablation was first demonstrated in 1960[2]. Since then, pulsed laser ablation has been studied on solid targets in vacuum and also in background gases, and is useful in the synthesis of nanoparticles and the fabrication of novel nanostructures.

In the process of nanosecond irradiation[27] of a solid target in a background gas, the ablation mechanism is mostly dominated by thermal processes[28]. A pulsed laser beam is focused on a target placed in a chamber filled with gas; and part of the laser energy is absorbed by the material near the surface. This laser-solid interaction, then results in a transfer of energy by heat conduction further into the interior of the target resulting in an immediate rise in temperature. The material near the surface undergoes melting, evaporation and eventually vaporization. When vaporization starts, a vapor plume expands. Due to a high temperature, a plasma is formed. As the laser beam decays, the plasma condenses in the background gas. Condensation can occur in two ways. One is the condensation of the plasma plume on a substrate placed near the solid, resulting in a thin film on the substrate. This method is called pulsed laser deposition. Second is the condensation of the plasma plume in the gas, which typically results in the formation of nanoparticles. This method is widely used in the synthesis of nanoparticles and the fabrication of nanostructures.

1.4.2 Laser ablation of solids in a liquid environment:

For pulsed laser ablation of a solid target in a liquid, a high energy density laser is focused onto the solid target and ablates the target at the liquid-solid interface as shown in figure 1.2. Pulsed laser ablation of a solid in a liquid environment was first demonstrated by

Patil and his co-workers in 1987[29]. They used a pulsed laser to ablate an iron target in water to form metastable phases of iron oxide.

The method of laser ablation in a liquid[17,30] to create nanoparticles has many advantages compared to conventional nanoparticles creation methods, such as chemical vapor deposition, laser ablation in vacuum or in a dilute gas. It is experimentally simple and chemically clean. The final product formed in this method is also highly pure. The high pressure, high temperature and resulting high energy density of this method are favorable for the formation of metastable phase[30], resulting in novel products.

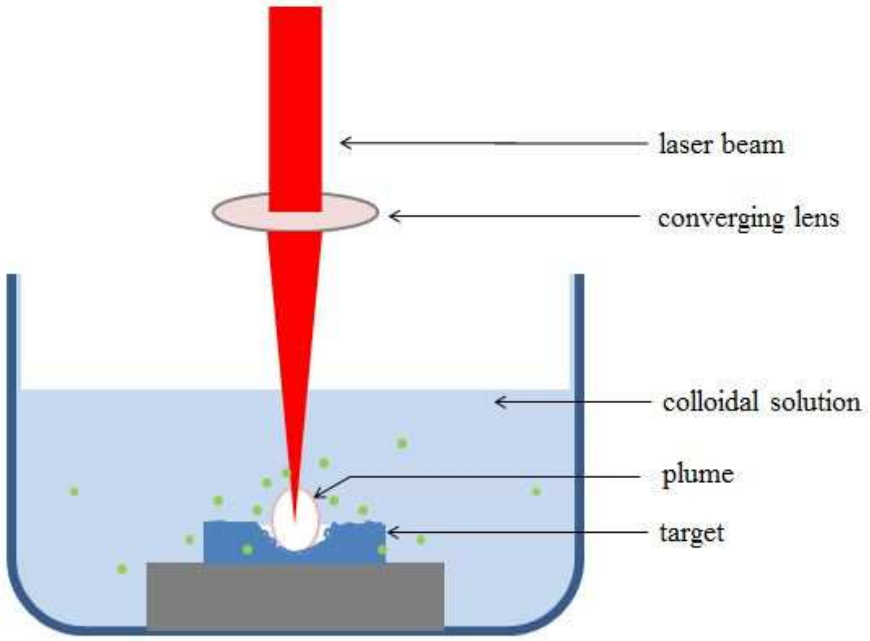

Figure 1.2: Schematic showing laser ablation of a solid in a liquid environment.

This technique also allows for the control of parameters, such as laser wavelength and fluence that affect the size and morphology[31,32] of the nanoparticles formed.

To have a clearer understanding of laser ablation of a solid in a transparent liquid, a brief summary of the physical phenomenon involved is discussed here. A high power pulsed laser is configured to be incident on the surface of the target placed in a liquid. The solid material absorbs a part of the laser energy and gets heated. Some of the absorbed laser energy is used to evaporate the target, thereby reducing energy transported into the interior of the target. The material that is ablated from the target leaves the target, expanding outward in the form of an ablation plume and creates a plasma[33]. The plasma may contain ions, electrons, atoms and clusters. Moreover, it may also contain liquid molecules or ions because the adjacent liquid also absorbs laser energy and may get ionized. It is possible that the plasma cloud may absorb some of the incident laser energy and thereby may allow only a fraction of the laser energy to reach the target surface. This is called plasma shielding[34]. The laser induced plasma plume expands and produces a shock wave in the liquid[35,36,37]. The shock wave also induces pressure in the plasma plume. Fabbro and his co-workers experimentally measured the pressure induced by the plasma with a neodymium glass laser of wavelength of 1060 nm and pulse widths of 3 ns and 30 ns[34]. They found the induced pressure of 5 GPa. The pressure inside the plasma plume is very high compared to atmospheric pressure. The pressure gradient causes expansion of the plasma plume which then quenches quickly. The high pressures, high temperatures and high energy densities are favorable for some chemical reactions to occur between the ablated species and confining liquid[30]. The result can be the formation of novel materials by the combination of elements of the target material and liquid.

1.5 Excimer laser:

Excimer lasers are pulsed gas lasers which emit in the UV spectral region. They were first invented by Nikolai Basov, VA Danilychev and Yu. M. Popov in 1970 at the Lebedev Physical Institute in Moscow[15]. The term 'excimer' is short for 'excited dimer'.

Excimer lasers use a halogen such as chlorine or fluorine, mixed with a noble gas such as argon, krypton or xenon, in the presence of buffer gas such as helium or neon. Noble gases are chemically inactive under normal conditions. However, under an appropriate electrical discharge or high-energy electron beams, which produce high energy pulses, a noble gas can be excited and ionized. The excited atoms can combine with themselves to form temporarily bound molecules (dimer) or with halogens (complexes). Typical excimer complexes include krypton fluoride (KrF), xenon fluoride (XeF), argon fluoride (ArF) and xenon chloride (XeCl). The excited states are short lived and when molecules transition into the ground state, the molecules dissociate into their elemental components. This process is accompanied by the release of the binding energy in the form of a photon, resulting in light in the UV region.

The pulse duration for an excimer laser is in the range 10-100 ns. This is a relatively short pulse length and leads to high peak power output. Excimer lasers can work at repetition rates from a single shot to a few kilohertz. Depending on the choice of excimer (F_2, ArF, KrF, XeCl, XeF), the laser can be operated at different wavelengths in the range 157-351 nm as shown in table 1.

Table 1: Excimer lasers and their wavelengths

Excimer	Wavelength (nm)
F_2	157
ArF	193
KrF	248
XeBr	282
XeCl	308
XeF	351

The pulse energy ranges from few millijoules to 300 millijoules. The beam obtained from an excimer laser has high power. This unique feature makes excimer laser useful for material removal. It is used to remove unnecessary parts and micro machine ceramics and semiconductors. It is also used to mark thermally sensitive material and in surgical operations. Excimer lasers applications are very broad with new area emerging continuously.

1.6 Nanotechnology and importance of nanoparticles:

Nanotechnology[26] deals with matter at the scale of one billionth of a meter. A nanoparticle is the fundamental component in the synthesis of nanostructures. According to the International Union of Pure and Applied Chemistry (IUPAC) definition, nanoparticles are particles of any shape with dimensions ranging between $1x10^{-9}$ m and $1x10^{-7}$ m. The prefix 'nano' comes from the Greek word 'nanos' which means dwarf. It is commonly used in the scientific literature.

Nanoparticles can have unusual and unique properties such as higher surface area, higher strength, different electronic structures and greater chemical reactivity compared to the bulk material. These novel properties cause them to be used in many applications, such as gas sensors[38], electrodes for solar cells[39], opto-electronic devices[40], and anti-microbial drug delivery[41]. Nanoparticles of GaAs, Si, and CdS, dispersed in glasses have been used in fast optical switches and optical fibers[42]. This thesis focuses on the production of tin and silicon nanoparticles in the absence and presence of electric fields and is motivated in part to find ways to tailor the properties of nanoparticles.

Silicon nanoparticles have many applications in biomedicine[43], optics and electronics. Mesoporous Si nanoparticles are being increasingly used in drug delivery systems[44] in the medical field. Their porous structures are used in electro-luminescent devices[45]. In addition, silicon thin films[46] can increase the output voltage of photovoltaic cells. Rong et al.[47] reported a co-axial silicon/anodic titanium oxide/silicon (Si-ATO-Si) nanotube array structure grown on a titanium substrate demonstrating the possibility of increasing the life span of lithium ion batteries and reducing recharge time.

Tin nanoparticles have been used as antibiotics, anti-fungal agents and for their anti-microbial properties[48]. Their semiconducting oxides (SnO_2) are extensively used in electrode materials, anti-reflection coatings in solar cells, photo-sensors and catalysts. They are also used in gas sensor technology[38,49]. Moreover, tin nanoparticle based materials can replace graphite electrodes in lithium batteries[50] leading to superior performance. They have countless applications with high demand in technological and commercial fields.

1.7 Laser ablation in a liquid assisted with an applied electric field:

During the process of laser ablation of a solid in a liquid, high temperatures and high pressures are attained. This causes ionization which is favorable for the formation of a plasma where molecules or atoms decompose into elemental components, electrons and ions. The charged species are affected by application of an electric field during the irradiation process, and may impact the particles produced during ablation. The electric field causes positively charged ions and electrons to drift in opposite directions, which will tend to disperse the plume. One result may be an increase in laser beam energy reaching the target surface. Moreover, the electric field can affect the phases, sizes and shapes of the nanoparticles as the surfaces of nanoparticles are charged. A.A.Serkov et al. demonstrated the influence of an applied electric field on laser ablation of titanium in water[51]. Similarly, Raid et al. showed the relation of particle size with the electric field applied during laser ablation of bismuth oxide (Bi_2O_3) in water.[52] The dependence of shape and size of the resulting nanoparticles on the applied electric field is of interest since this holds promise as a way to control nanoparticle manufacturing.

CHAPTER 2

THEORY

2.1 Interaction of light with material:

When light interacts with matter, a complicated light-matter dynamic occurs. In general, when light is incident upon a material, three effects occur: reflection, absorption and transmission. Because light is a form of energy, the conservation of energy tells us that

$$I_o = I_R + I_A + I_T \tag{2.1}$$

where I_o is intensity of incident light and I_R, I_A and I_T are the intensities of the light reflected, absorbed and transmitted, respectively.

An alternative form of equation (2.1) is

$$R + \alpha + T = 1 \tag{2.2}$$

where R, α and T represent reflectivity (I_R/I_o), absorptivity (I_A/I_o), and transmissivity (I_T/I_o) respectively.

For an opaque material,

$$R + \alpha = 1 \tag{2.3}$$

In the laser ablation process, the optical properties of the solid material determine the absorption and reflection of light impinging on it. It is characterized by an optical quantity called the complex refractive index which is wavelength dependent. The complex refractive index[53] N with real and imaginary parts n and k is

$$N = n + ik \tag{2.4}$$

where n is the real part of the refractive index and is often called the refractive index and k is the imaginary part of complex refractive index and is called the extinction coefficient. The

extinction coefficient is related to the absorption of light by the material. The refractive index of a material is related to its dielectric constant. The complex dielectric constant[53] ε with real and imaginary parts ε_1 and ε_2 is given by

$$\varepsilon = \varepsilon_1 + i\varepsilon_2 \tag{2.5}$$

The complex refractive index is related to its dielectric function by

$$N = \sqrt{\mu\varepsilon} \tag{2.6}$$

where μ is the magnetic permeability of the medium. For a non-magnetic material such as silicon or tin, μ is 1. The complex dielectric function is then

$$\varepsilon = (n + ik)^2 \tag{2.7}$$

This yields (with $\mu = 1$)

$$n = \sqrt{\sqrt{\frac{\varepsilon_1^2+\varepsilon_2^2}{2}} + \frac{\varepsilon_1}{2}} \tag{2.8}$$

$$k = \sqrt{\sqrt{\frac{\varepsilon_1^2+\varepsilon_2^2}{2}} - \frac{\varepsilon_1}{2}} \tag{2.9}$$

David W. Lynch and W R Hunter reported the value of n and k for tin at the wavelength of 351 nm are 0.9 and 3 respectively and for silicon at the wavelength of 351nm, they are 5.4679 and 1.6359 respectively.[54]

The extinction coefficient (k) describes the attenuation of light in a material. This phenomenon is well explained by the Beer-Lambert law.[55] This law gives an expression for the absorption of incident light and tells us that the intensity of light decreases exponentially with depth in the material. The equation is

$$I(x) = I_o e^{-\alpha x} \tag{2.10}$$

where I_o is the intensity of the incident light falling on the target surface and x is the depth through which light passes in the material. The absorption coefficient (α) and extinction coefficient are related by

$$\alpha = \frac{4\pi k}{\lambda} \ (\text{cm}^{-1}) \tag{2.11}$$

where λ is the wavelength of light. Corresponding to the wavelength 351 nm, the value of extinction coefficient 'k' for tin and silicon are listed above and the absorption coefficient, α, can be calculated using equation (2.11).

In laser ablation of a solid in a liquid environment, the laser beam passes through the liquid-solid interface. The amount of light absorbed in laser ablation by an opaque material is related to the reflectivity at the front surface of solid material. The reflection coefficient R[56] of an interface between liquid and solid is given by

$$R_{ls} = \left|\frac{N_l - N_s}{N_l + N_s}\right|^2 = \frac{(n_l - n_s)^2 + (k_l - k_s)^2}{(n_l + n_s)^2 + (k_l + k_s)^2} \tag{2.12}$$

For efficient laser ablation, the reflectivity at the solid-liquid interface should be low for the absorption to be higher. Since liquids have higher refractive indices compared to gases, there is a reduced reflection for ablation performed in liquid environment. However, the absorption of light by the liquid layer is typically greater than for a gas, which would tend to reduce the laser beam intensity at the target surface for ablation in liquid, as compared to gas. In our experiment, the upper surface of the solid target placed in water has a thickness of water of 2 cm above it in order to get the highest ablation rate.

2.2 Thermal effects of laser in ablation:

We can describe the interaction of a nanosecond laser pulse with a solid as a thermal process. Several authors (Wood and Giles[57], Singh R K and Narayan[58], Boardman *et al*[59],

Amoruso[60]) have modeled the laser-solid interaction in the nanosecond regime. It results in heating of the material, melting, vaporization, plasma expansion and phase explosion.

2.2.1 Heating and melting:

During the ablation process, a significant part of the energy of laser irradiation is converted into heat. The heat energy is absorbed and is stored in a layer with a thickness of the order of L_{th}, where L_{th} is the heat penetration depth[28] and is given by $L_{th} \approx (2D\tau_p)^{1/2}$ with τ_p being the laser pulse duration and D being the heat diffusion coefficient, which is related to thermal conductivity (k) and specific heat (C_p) by $D = k/\rho C_p$. Heat conduction in the solid is governed by the heat diffusion equation based on the Fourier law of conduction[61].

$$\rho C_p \frac{\partial T(z,t)}{\partial t} = \frac{\partial}{\partial z}\left[k \frac{\partial T(z,t)}{\partial z}\right] + \alpha(1 - R) I_0(t) e^{-\alpha z} \qquad (2.13)$$

where, ρ is the density, C_p is the specific heat, T is the temperature at depth z at time t, R is the reflectivity of the surface, α is the absorption coefficient and $I_o(t)$ is the laser irradiance. The term on the left hand side represents the rate of flow of heat per unit volume into the material. The first term in the right hand side represents the heat flow out of the material and the second term shows that the optical intensity decays exponentially inside the material.

At the very beginning of the laser-material interaction, the temperature of the target is below the melting point. After some time when the temperature at a certain depth in the target material exceeds the melting point, melting of the target material starts. The temperature remains constant during the time the phase transition (melting) occurs. The boundary condition is

$$T_s(z = z_i) = T_l(z = z_i) = T_m \qquad (2.14)$$

where T represents the temperature with suffices s, *l*, and m corresponding to solid, liquid and melting respectively.

The energy balance equation[62] is

$$K_s\frac{\partial T_s}{\partial z} - K_l\frac{\partial T_l}{\partial z} = h_{sl}V_i \tag{2.15}$$

where h_{sl} is the latent heat for melting and V_i is the interface velocity.

For surface melting, the interface velocity[61] is given by

$$V_i = B(T_m - T_i) \tag{2.16}$$

where T_m and T_i are the melting and interface temperatures respectively, and B is the kinetic melting coefficient.

2.2.2 Vaporization:

Primarily, the surface temperature determines the vaporization rate. During a laser-matter interaction, when the surface temperature reaches the boiling point, vaporization becomes significant. The molten material starts evaporating and forms a Knudsen layer near the ablative material where evaporating particles reach thermal equilibrium after collisions. The vaporization rate[63] from the surface of molten material is given by

$$J_v = n_l\left(\frac{k_B T_l}{2\pi m_a}\right)^{1/2}\exp\left(-\frac{h_v}{k_B T_l}\right) - \theta_s n_v\left(\frac{k_B T_v}{2\pi m_a}\right)^{1/2} \tag{2.17}$$

where, n is the number of atoms per unit volume and subscripts *l* and v represent the liquid and vapor respectively, h_v is the latent heat of vaporization, T_v is the temperature of the vapor, m_a is the atomic mass and k_B is the Boltzmann constant. The first term in the right hand side represents the rate of evaporation from a liquid surface. The second term in the

equation (2.17) represents the condensation rate of molecules back to the liquid surface with θ_s being the probability of a vapor atom returning to the liquid surface.

The vapor pressure is determined using the Clausius–Clapeyron equation[64].

$$P_s = P_o \exp\left(\frac{H_v(T-T_b)}{RTT_b}\right) \tag{2.18}$$

where H_v is the enthalpy of vaporization, T is the temperature of the liquid surface, T_b is the boiling temperature, and P_o is ambient pressure.

2.2.3 Phase explosion:

With sufficiently high laser fluence, the temperature of the molten material can be higher than the vaporization temperature, creating a superheated liquid layer. When this is superheated, the heating process shifts away from the binodal into the metastable region and follows a superheating line approaching the spinodal as in figure[64] 2.1. The region between the binodal and spinodal is the region of the metastable state.

The spinodal is the limit of phase stability and is determined from the Gibbs' potential[64] as

$$\left(\frac{\partial P}{\partial V}\right)_T = 0 \tag{2.19}$$

where V is the specific volume. As the temperature approaches the spinodal, the thermodynamic properties of the material change dramatically. There are large fluctuations in the density of the material which result in the nucleation of bubbles. The rate of nucleation can be determined from Döring and Volmer's theory[64]. According to this theory, if the heating rate is slow, the frequency of nucleation is given by

$$J = N\left(\frac{3\sigma}{\pi m}\right)^{1/2} \exp\left(\frac{-W_{cr}}{K_B T}\right) \tag{2.20}$$

where W_{cr} is the energy needed for the formation of nuclei at temperature T, N is the number of liquid molecules per unit volume and σ is the surface tension.

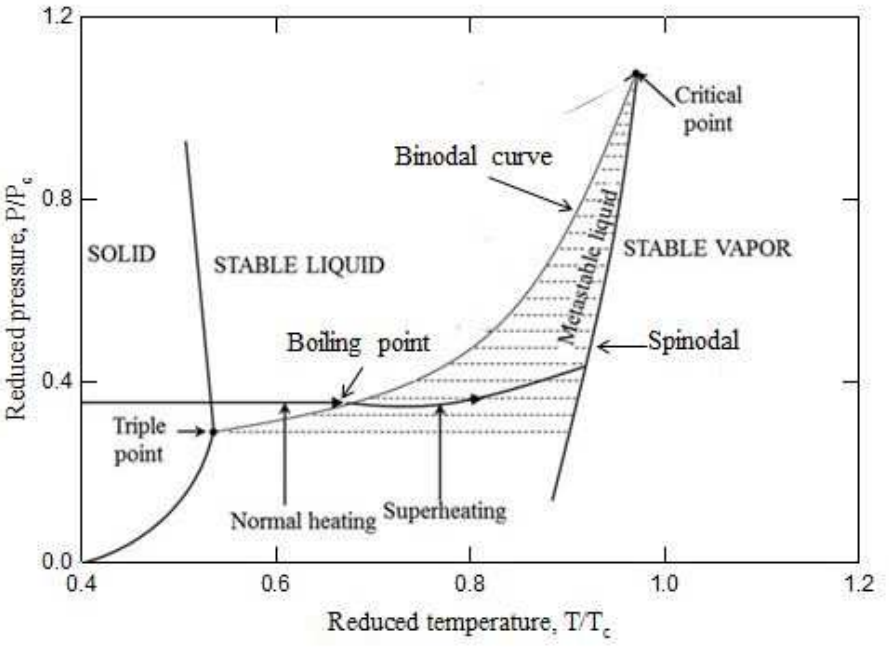

Figure 2.1: Pressure-Temperature diagram with binodal and spinodal curves.
(Source: Non-equilibrium phase change in metal induced by nanosecond pulsed laser ablation; Xianfan Xu, 2002[64].)

For a slowly heated liquid, spontaneous nucleation causes a homogeneous phase change at the normal boiling point. Therefore, a superheated state cannot be sustained. For a quickly heated liquid, the liquid moves into the metastable region, approaches the spinodal and experiences spontaneous nucleation.

At a temperature of about 0.9 T_c (T_c is the critical temperature) significant numbers of cavitation bubbles are formed and continuously expand in the superheated liquid. The plume expansion and formation of a higher pressure region above the solid surface exerts a recoil pressure on the underlying melt. Such high pressure acting on the surface might give rise to a piston effect on the molten layer. This causes the ejection of the melted material from the

irradiated region. In this case, the molten material splashes into fragments and droplets and comes out of the surface explosively, which is termed as phase explosion or explosive boiling. After the explosion, the material fragments go into the surrounding liquid medium.

2.3 Formation of nanoparticles:

During pulsed laser irradiation of a solid in liquid confinement, nanoparticles with the sizes ranging from 1 nm to few hundred nanometers are fabricated. In our experiments of laser irradiation of tin and silicon in a water environment, most of the nanoparticles produced had sizes from 1 nm to several tens of nanometers. We also found some particles with sizes above 100 nm. We can categorize the size of particles into three groups: small nanoparticles, intermediate nanoparticles and big particles with the range of sizes 1-10 nm, tens of nanometers and hundreds of nanometers, respectively.

When a sufficiently intense laser beam is incident on a solid target, the top surface of the solid material melts and the molten material nucleates homogeneously[65]. The vapor plume produced may contain ions, atoms and clusters of both the liquid and solid. In phase explosion[64], the vapor plume and liquid droplets of molten material move outward almost radially away from the surface of the solid. This expansion in the surrounding liquid results in its quench. The condensation of the vaporized atoms and droplets is considered as an effective mechanism for the formation of small nanoparticles. During the process, some of the nanoparticles continue to grow by capturing surrounding atoms and nuclei in the vapor and therefore, form bigger nanoparticles which are categorized as intermediate nanoparticles in this thesis. The pressure, temperature and the nature of liquid and target are the main factors that determine the quenching or condensation process.

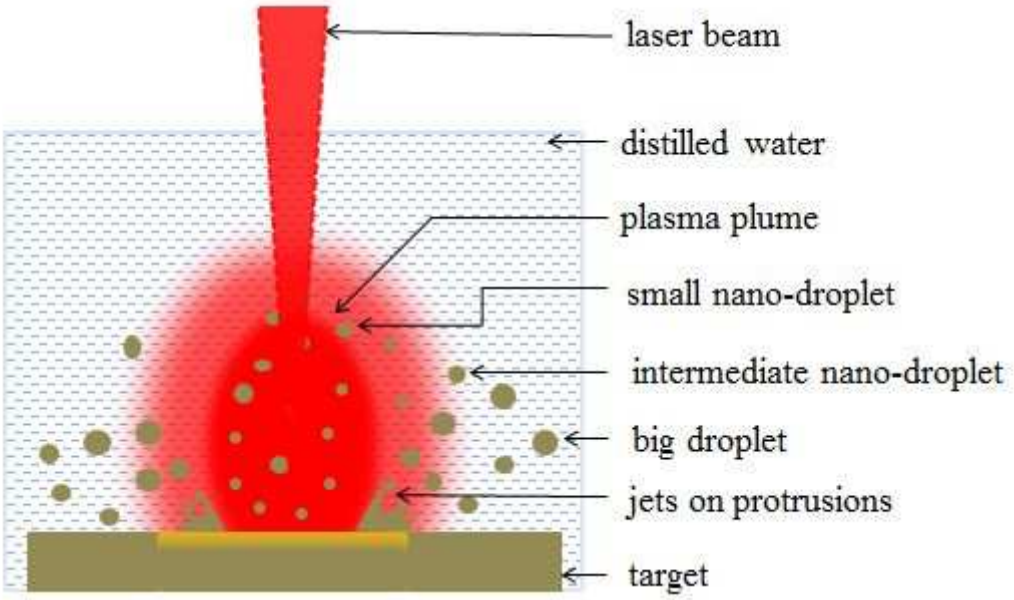

Figure 2.2: Simple mechanism depicting formation of nanoparticles.

Furthermore, the expansion of the molten material is in the radial direction to the surface forming protrusions.[66] At the tip of protrusions, jets of droplet-vapor mix are formed due to the high pressure and surface tension of the liquid material. The jets detach from the base and break up into droplets as shown in figure 2.2. The Rayleigh-Plateau instability[66] is responsible for the formation of liquid jets breaking into droplets. The particles formed through this process are bigger[67] up to one micron. Besides this, there may be some other mechanisms like solid exfoliation, spallation and hydrodynamic sputtering which can describe the generation of large sized particles.

2.4 Method of calculating particle size:

Once we confirm the formation of nanoparticles in the TEM images, it is a great challenge for us to determine their sizes accurately. In the TEM images, we find particles are of same shape with varying sizes. Most of the particles overlap which may cause difficulty in determining size. There are various software packages like ImageJ, Dizimizer, Irfan view and MS paint which can be employed to determine the size of particles from a TEM image.

We used 'MS paint' in order to calculate each particle's size. Since the nanoparticles formed were spherical in shape, we used the relation

$$\text{Particle size} = \mathrm{P}x_p * \left(\frac{\mathrm{L}_s}{\mathrm{P}x_s}\right) \tag{2.21}$$

where $\mathrm{P}x_p$ represents the length in pixels of the particle, $\mathrm{P}x_s$ represents the length, in pixels, of the scale and $\mathrm{L_s}$ is the actual length of the scale indicated in the TEM image.

We calculated the difference in the pixels either horizontally or vertically as in figure 2.3 for all the particles that were chosen. As shown in figure 2.3, the pixel width of the particle diameter is 961-729=232; the pixel width of the scale is 1165-705=460; and the length of the scale is 50 nm. These values, upon substitution in equation 2.22, give the size of the particle to be 29 nm. Use of MS Excel made it easier to calculate the average size and standard deviation of nanoparticles.

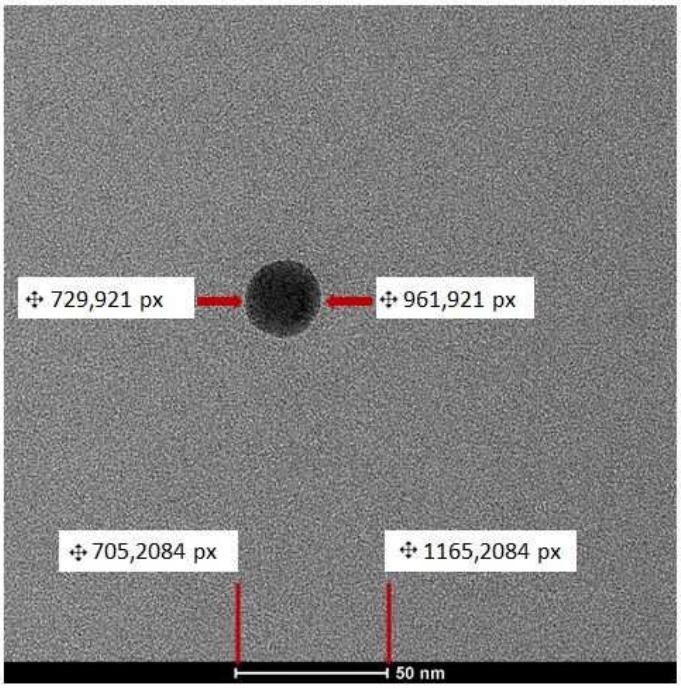

Figure 2.3: Calculation of particle size by determining the pixel width.

CHAPTER 3

EXPERIMENT

3.1 Experimental procedure:

The laser used for ablation of both tin and silicon was a Coherent COMPex PRO 201F XeF excimer laser operating at a wavelength of 351 nm with 25 ns pulses. The whole experimental procedure was categorized into three sections, each section explained in detail below.

3.1.1 Pre – ablation procedure:

Prior to the ablation process, a series of procedures like sample preparation, cuvette cleaning and arranging the equipment was performed. A quartz cuvette of dimensions 5.0 cm x 5.0 cm x 2.0 cm was washed using ethanol in order to remove dust and particles. It was then rinsed 3-4 times with distilled water which was also used as liquid confinement.

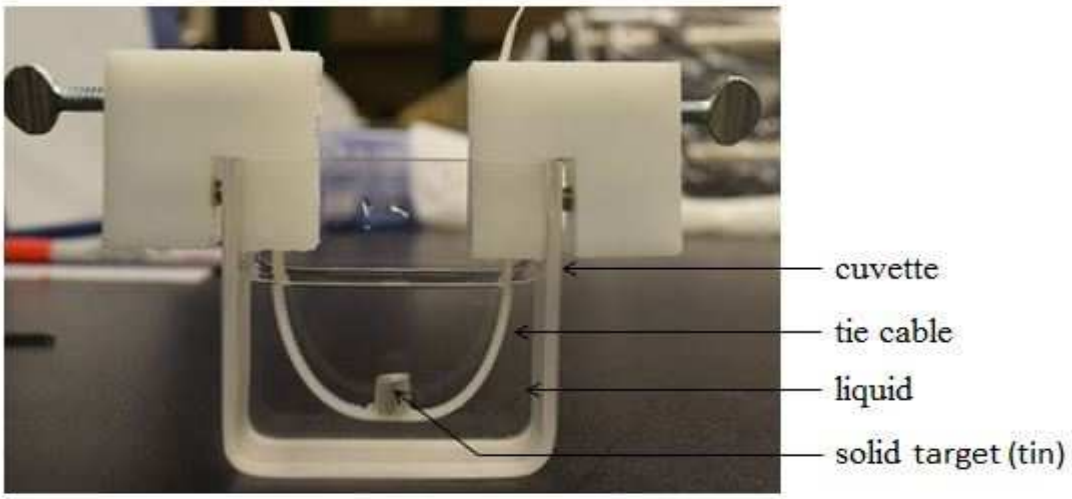

Figure 3.1: Target glued to a plastic tie and positioned inside the cuvette in liquid.

For the irradiation of tin, a small cylindrical shaped tin piece (purity > 99%, length 7 mm) was glued to a plastic cable tie. The tin piece (target) glued to the plastic tie was rinsed several times and was positioned inside the cuvette filled with distilled water for the irradiation as shown in figure 3.1. For the irradiation of the silicon target, the sample was prepared in a similar way and also ablated in distilled water.

3.1.2 Laser irradiation procedure:

After the sample was ready, the next step was to irradiate it with the laser beam. Figure 3.2 shows a schematic diagram of irradiation of a target. The laser pulse duration was 25 ns, the repetition rate for tin was 2 Hz and for silicon, it was 1 Hz. The diameter of the laser spot on the target's surface was 60 μm. The target surface was approximately 2 cm below the surface of the liquid in the cuvette. The laser fluence was 62 J/cm^2 for the ablation of tin, and for silicon, it was 128 J/cm^2.

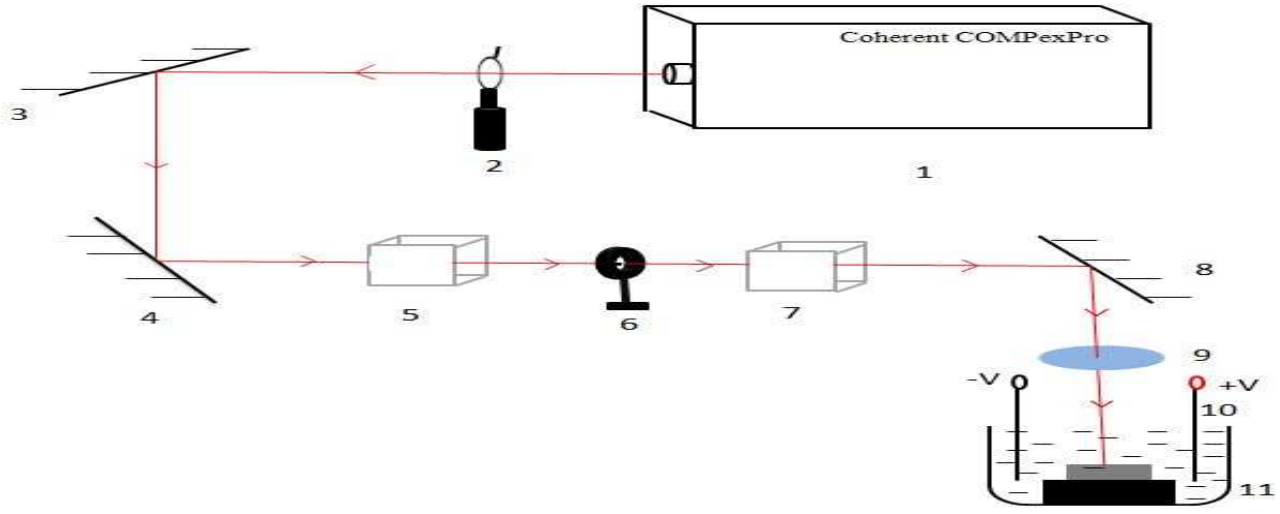

Figure 3.2: Schematic diagram of laser ablation of a solid in a liquid. In the diagram, the numbers represent: 1-Excimer laser; 2-aperture; 3,4-mirrors; 5,7-polarizing beam splitter; 6-half wave plate; 8-mirror; 9-focusing lens; 10-electrodes; 11-target supported in cuvette.

The laser beam first passes through an aperture. After reflecting off of mirrors, it passes through polarizing beam splitter, a rotating zero order half wave plate and then another polarizing beam splitter. The polarizing beam splitter-half wave plate-polarizing beam splitter combination works as an optical attenuator. The experimental arrangement is shown in figure 3.3.

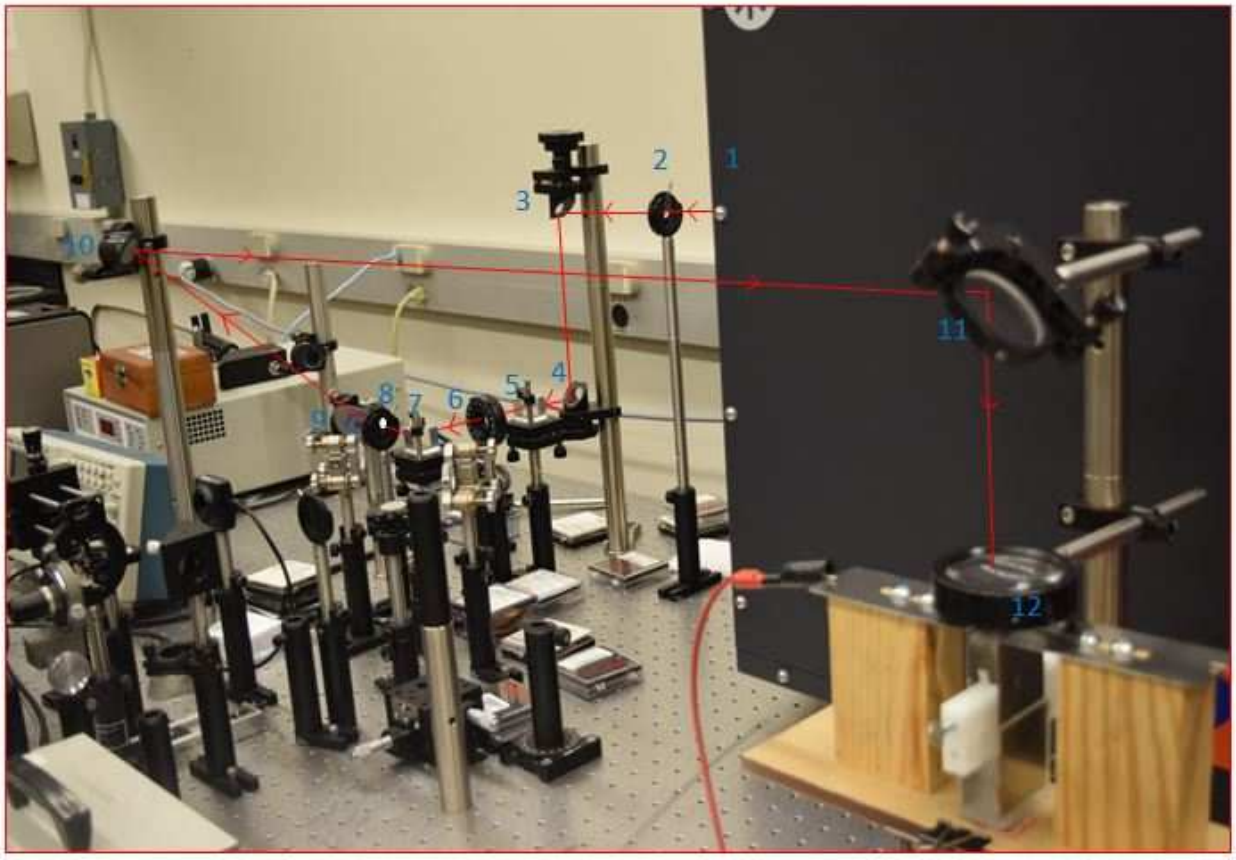

Figure 3.3: Experimental setup in the lab for the laser ablation of a solid in a liquid. In figure, 1: laser; 2, 8: apertures; 3, 4: mirrors; 5, 7: polarizing beam splitters; 6: half wave plate; 9, 10, 11: mirrors and 12: converging lens.

A converging lens was used to focus the laser onto the target. The tie with a target glued at its middle was fixed to the two edges of the cuvette. The cuvette was then placed

onto a lab jack. The lab jack was movable in the vertical direction and adjusted to bring the target to the focus of the lens.

To study the influence of electric fields in the fabrication of nanoparticles of tin, electric potential differences were applied with the help of two metallic electrodes. The electrodes were placed in water and a distance of 2 cm was kept between them throughout the experiment, as shown in figure 3.3. For the case of irradiation of silicon, five different potential differences of 0V, 5V, 10V, 15V and 18V were applied. The sample was held near the middle of the two parallel electrodes. The magnitude of the electric fields applied for the irradiation of tin were 0 V/cm, 2.5 V/cm, 5 V/cm and 9 V/cm and for the irradiation of silicon, they were 0 V/cm, 2.5 V/cm, 5 V/cm, 7.5 V/cm and 9 V/cm.

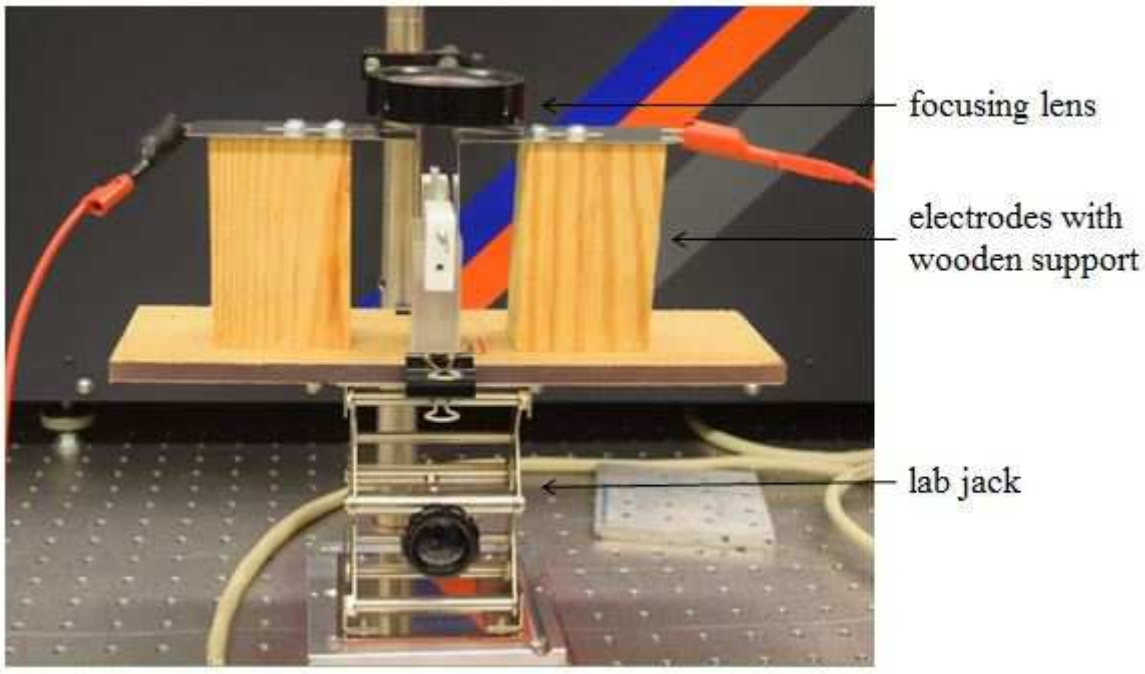

Figure 3.4: Arrangement of electrodes.

3.1.3 Post – ablation procedure:

After the irradiation of tin/silicon for about 20/30 minutes at a repetition rate of 2/1 Hz, about 10 ml of the resulting colloidal solution was poured into a small glass beaker. The formation of nanoparticles in the solution could be confirmed by passing laser light through the solution. If the path of laser light was seen distinctly, we could assume the presence of nanoparticles in the solution which caused scattering of light. A transmission electron microscope specimen grid was put on the bottom of a beaker with the dark side facing up. In this experiment, the TEM grid used was 3 mm in diameter and 400 mesh copper grids coated on one side with a 20 nm thin film of amorphous carbon (dark side of grid) on the other side. The beaker was then placed under a hood to allow the liquid to evaporate at room temperature. This took several days.

For this thesis, after the ablation products of tin were deposited on the TEM grid, the grid was put in the petri dishes and was sent to the TEM Operator in School of Dentistry, UMKC. He used a Scanning Transmission Electron Microscope CM12 operating between 20 to 120kV. TEM samples of silicon were sent to the TEM Operator, Material Research Center in Missouri S & T, Rolla. She used a FEI Tecnai F20 TEM to study the sample. Imaging was done at 200 kV using a single tilt holder.

CHAPTER 4

ANALYSIS OF COLLECTED DATA

4.1 Results:

We analyzed the data obtained from the laser ablation of silicon and tin carried out in distilled water under different applied electric fields leading to the formation of nanoparticles of different sizes.

4.1.1 Fabrication of tin nanoparticles:

Experimental results obtained from the TEM images revealed particles with sizes from 1 nm to several hundred of nanometers. The reasons for this have already been discussed in the previous section (2.3). We have categorized the nanoparticles into two categories; small nanoparticles with size ranging in 1-10 nm and intermediate nanoparticles with size of tens of nanometers. Very few particles were found to have size bigger than 100 nm. We have categorized them as big particles. TEM images with the corresponding particle size distribution (figure 4.1 to 4.16) showed that the size of nanoparticles formed was different at different applied electric fields. This confirms the influence of electric fields applied externally on the formation of nanoparticles during the laser ablation of tin. We found the size of nanoparticles decreases with increasing electric field. The shape of nanoparticles formed was spherical at all applied electric fields as seen in the TEM images. We did not notice any significant change in morphology of particles at different electric fields with maximum at 9 V/cm. The experimental conditions and the results were summarized in the table 2.

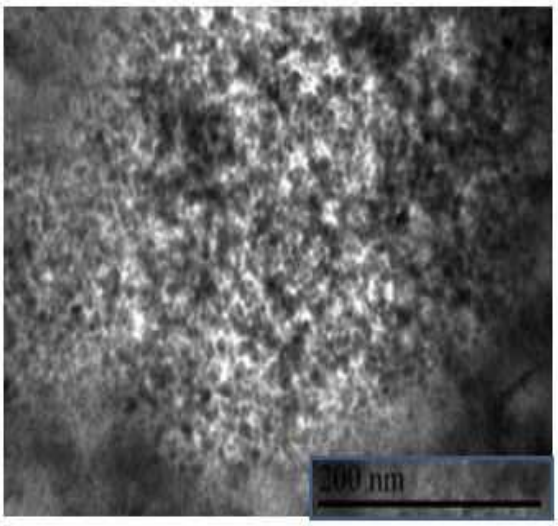

Figure 4.1: TEM image of small nano-particles of tin ablated in water when no electric field is applied.

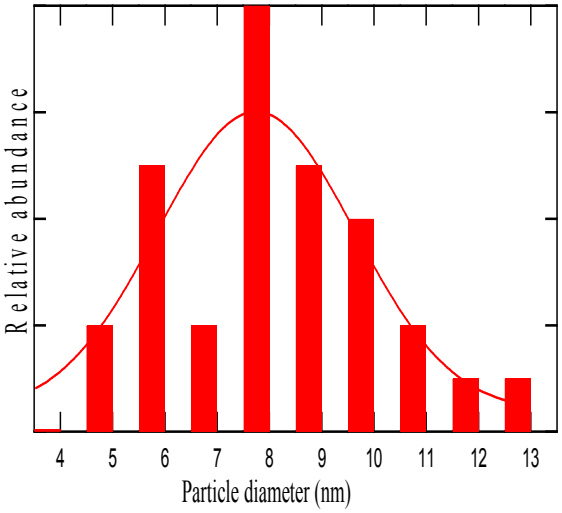

Figure 4.2: Particle distribution of the tin nanoparticles corresponding to Fig.4.1

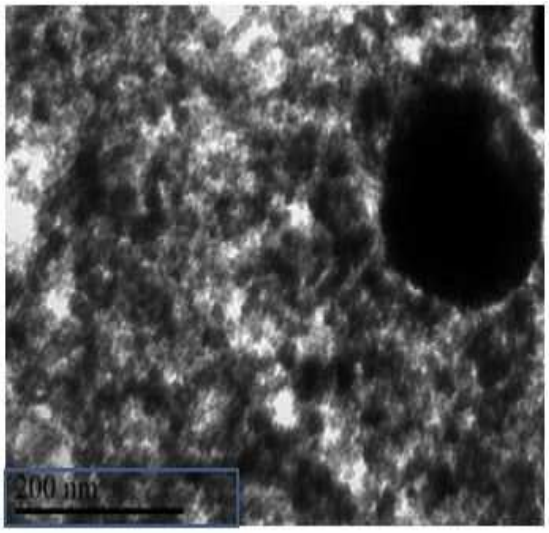

Figure 4.3: TEM image of small nano-particles of tin ablated in water at 2.5 V/cm.

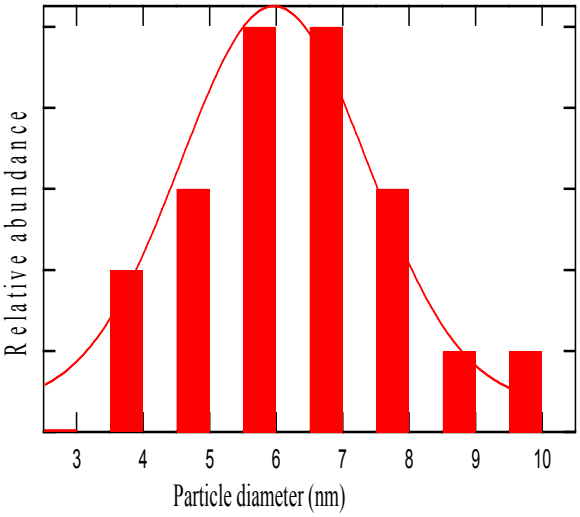

Figure 4.4: Particle distribution of the tin nanoparticles corresponding to Fig.4.3.

Table 2: Summary of experiment of laser irradiation of tin in water:

S.No.	Electric Field (V/cm)	Average size of small nanoparticles (nm)	Average size of intermediate nanoparticles (nm)	Average size of big particles (nm)
1	0	8 ± 2	40 ± 6	600 ± 160
2	2.5	6.5 ± 1.5	28 ± 4	425 ± 45
3	5	5 ± 2	22 ± 3	-
4	9	4 ± 1	14 ± 4	275 ± 130

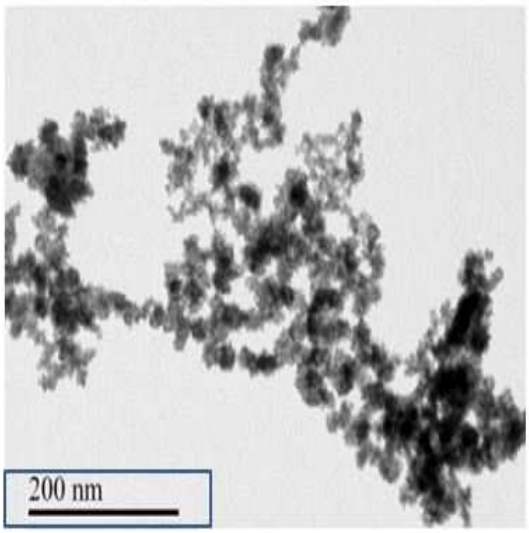

Figure 4.5: TEM image of small nano-particles of tin ablated in water at 5 V/cm.

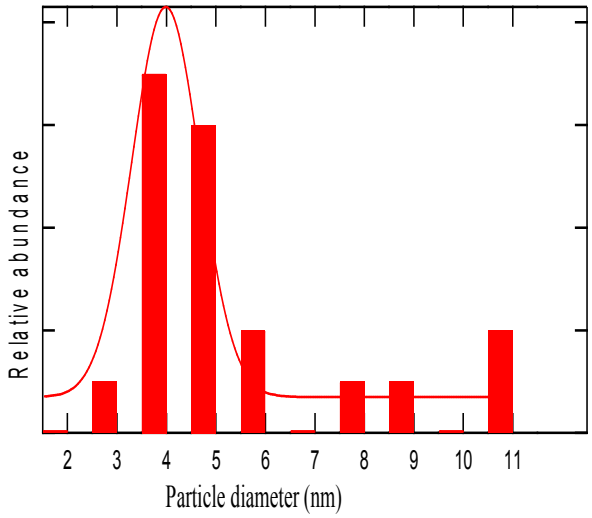

Figure 4.6: Particle distribution of the tin nanoparticles corresponding to Fig.4.5.

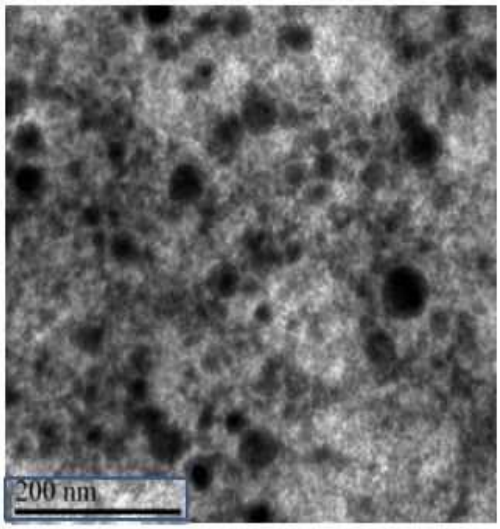

Figure 4.7: TEM image of small nano-particles of tin ablated in water at 9 V/cm.

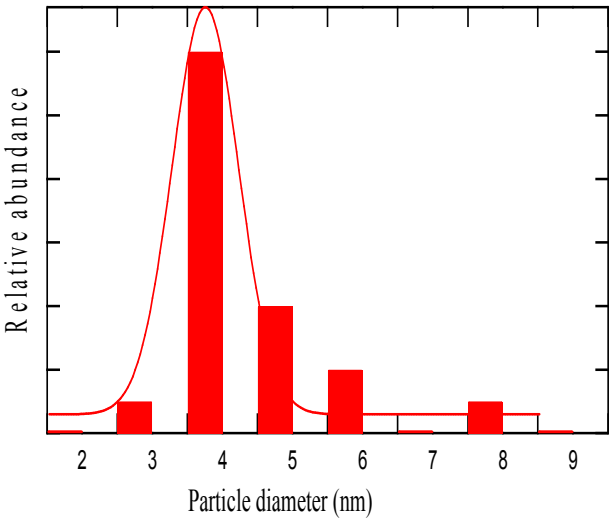

Figure 4.8: Particle distribution of the tin nanoparticles corresponding to Fig.4.7.

TEM images (Fig.4.1, 4.3, 4.5, and 4.7) depict the presence of both small nanoparticles and intermediate nanoparticles. We calculated the average sizes of small nanoparticles and plotted the particle distribution. Fig. 4.2, 4.4, 4.6, and 4.8 are the particle size distributions corresponding to the nanoparticles in Fig. 4.1, 4.3, 4.5, and 4.7 respectively.

We also calculated the average sizes of the intermediate nanoparticles. Different TEM images obtained at different applied electric fields are helpful in calculating the sizes of nanoparticles and investigating the relation of their sizes with the applied fields.

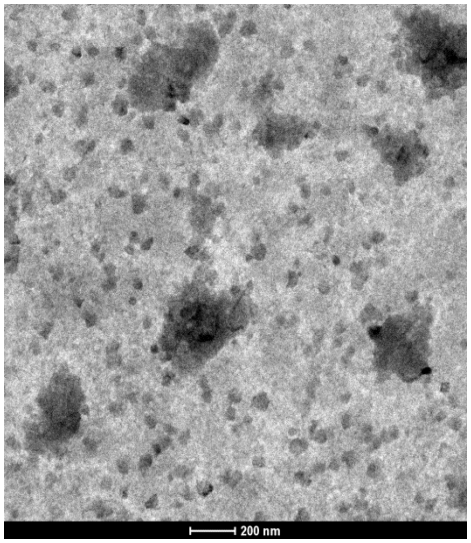

Figure 4.9: TEM image of intermediate nanoparticles of tin ablated in water when no electric field was applied.

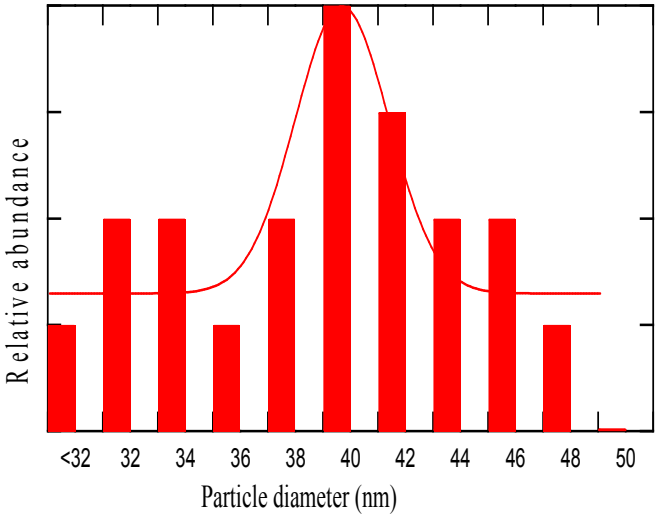

Figure 4.10: Particle distribution of tin nanoparticles corresponding to Fig. 4.9.

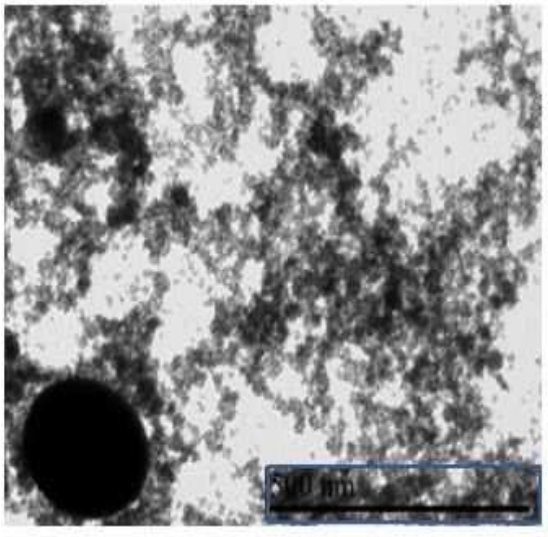

Figure 4.11: TEM image of intermediate nanoparticles of tin ablated in water at 2.5 V/cm.

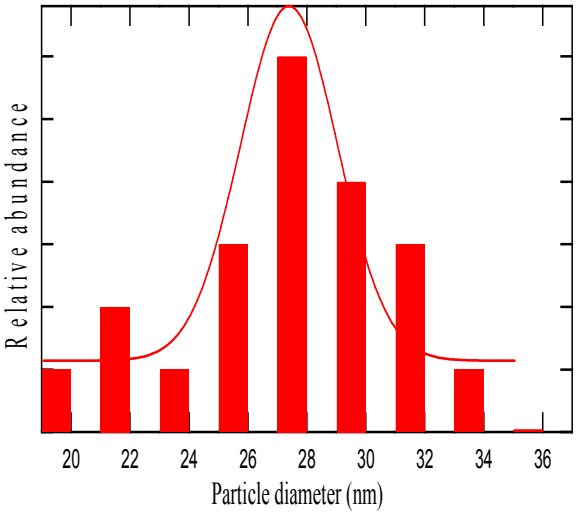

Figure 4.12: Particle distribution of tin nanoparticles corresponding to Fig.4.11.

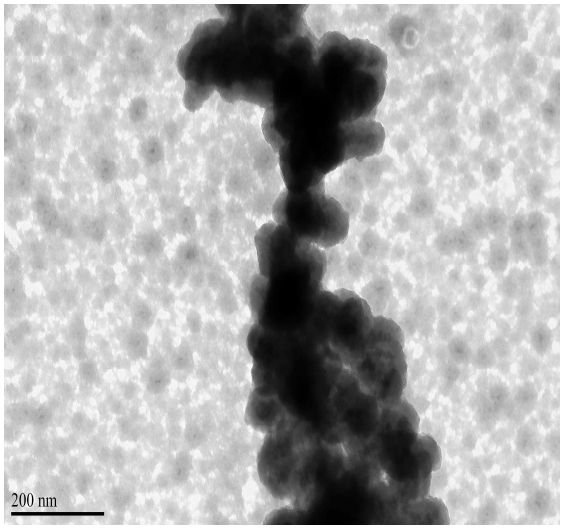

Figure 4.13: TEM image of intermediate nanoparticles of tin ablated in water at 5 V/cm.

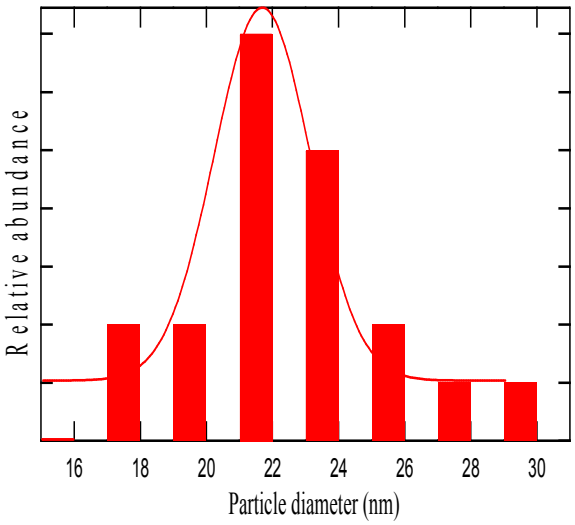

Figure 4.14: Particle distribution of tin nanoparticles corresponding to Fig. 4.13.

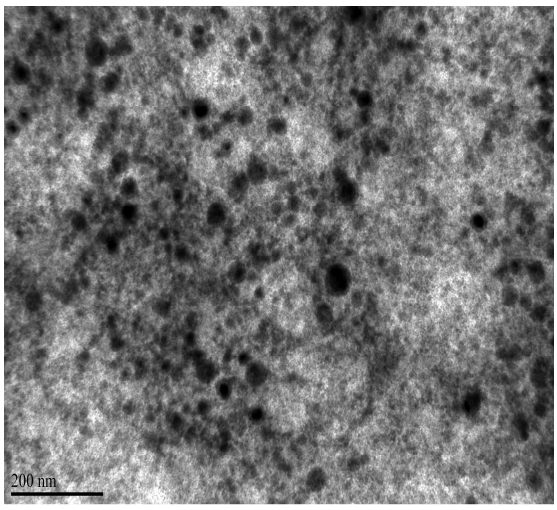

Figure 4.15: TEM image of intermediate nanoparticles of tin ablated in water at 9 V/cm.

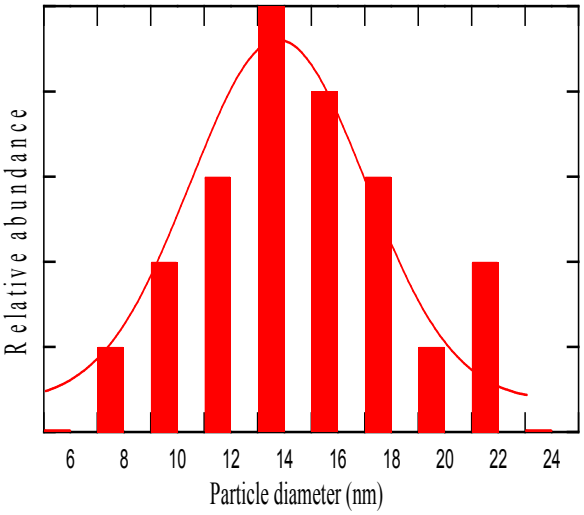

Figure 4.16: Particle distribution of tin nanoparticles corresponding to Fig. 4.15.

We see that there were few very big nanoparticles of the sizes of hundreds of nanometers formed during the laser ablation of tin in water. There are few protrusions with the jets on the target surface formed during the process of ablation. These jets detach from the base and remain in the liquid in the form of droplets.This might be because of Rayleigh-Plateau instability as discussed in the previous section (2.3). These droplets give rise to the big particles. In figure 4.17, the black spots are the clusters or the big particles formed during the process of ablation.

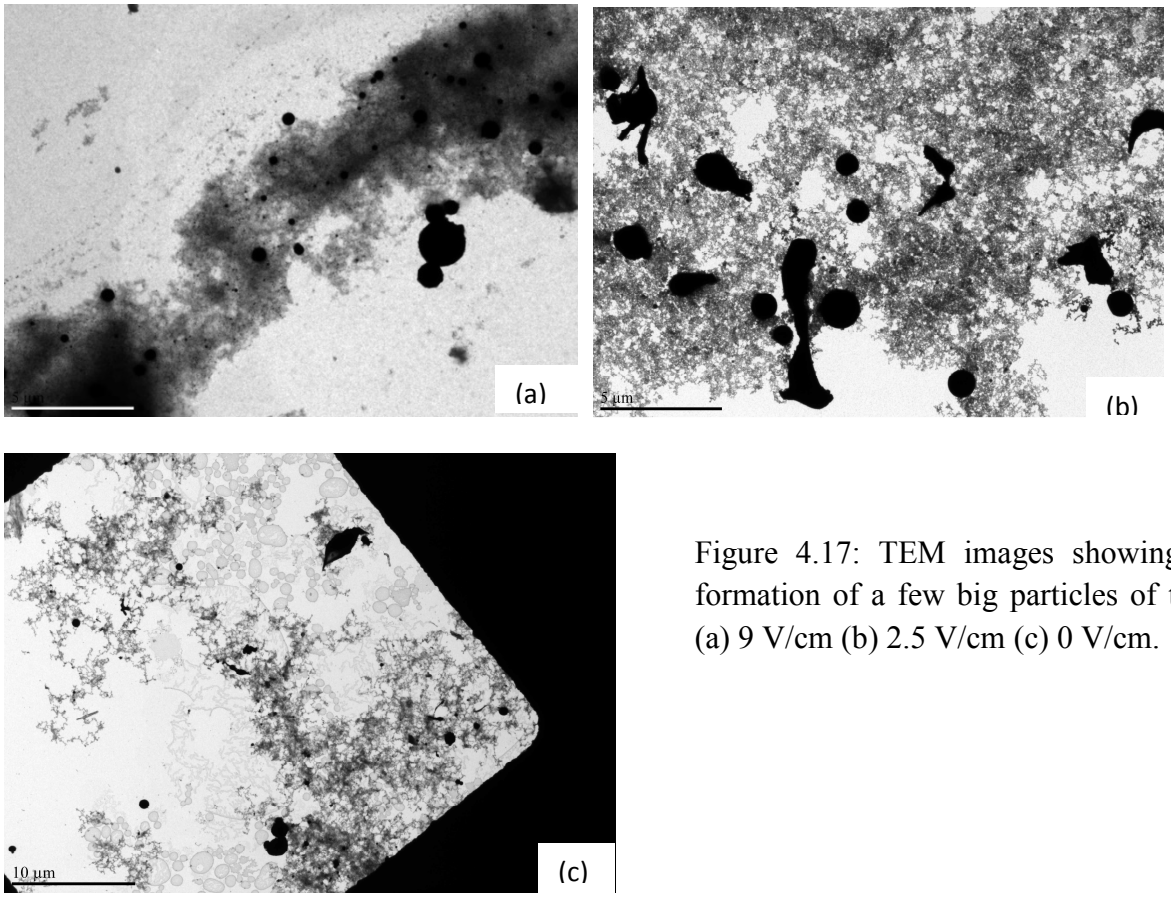

Figure 4.17: TEM images showing the formation of a few big particles of tin at (a) 9 V/cm (b) 2.5 V/cm (c) 0 V/cm.

Analysing the data collected in table 2 for the small and intermediate nanoparticles, we found that the sizes of nanoparticles depended on the applied electric field. The graphs plotted (figure 4.18, 4.19) for the data in table 2 for small and intermediate nanoparticles show that the particle sizes decrease with increase in the applied electric field.

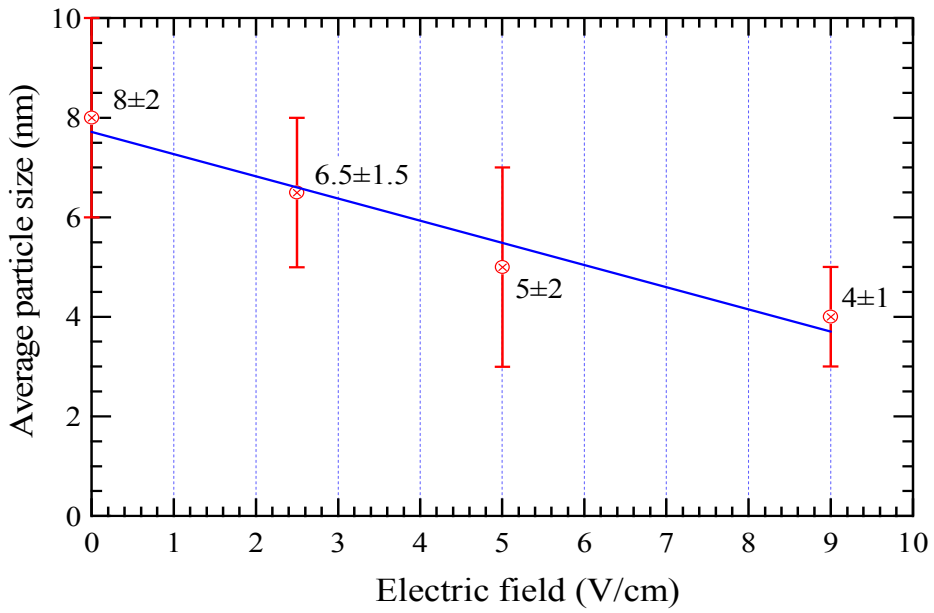

Figure 4.18: Graph of average particle size versus applied voltage for the data collected in table 2 for small nanoparticles of the tin. The blue line is the line of best fit y = a + bx with a = 7.71± 0.36 and b = -0.44±0.07.

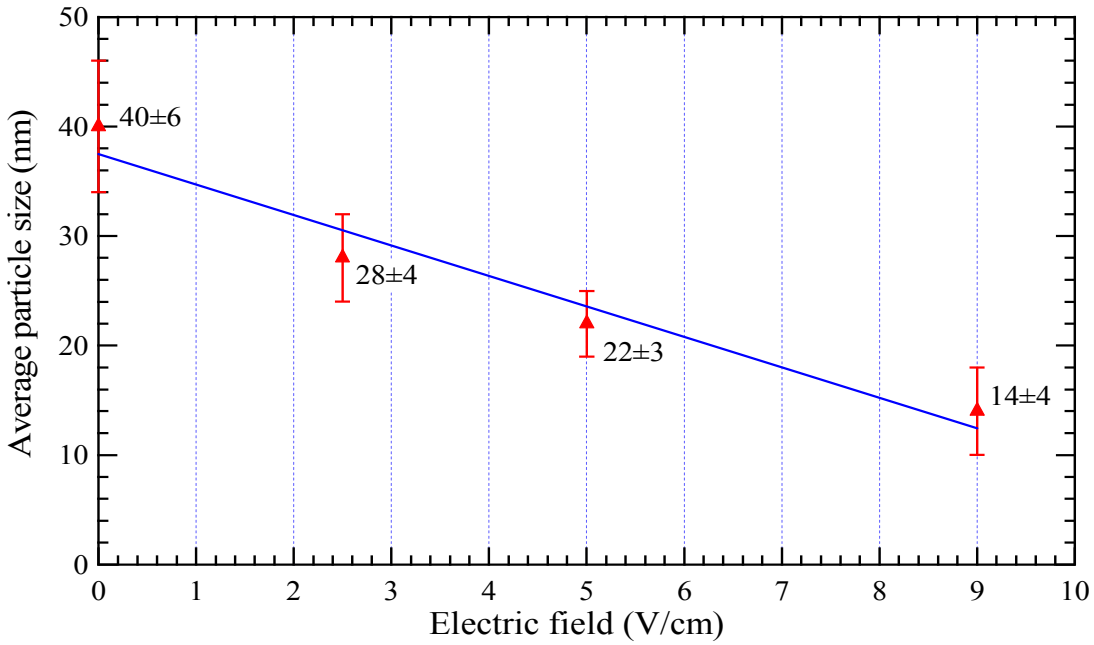

Figure 4.19: Graph of average particle size versus applied voltage for the data collected in table 2 for intermediate nanoparticles of the tin. The blue line is the line of best fit y = a + bx with a = 37.48± 2.37 and b = -2.78±0.44.

4.1.2 Fabrication of silicon nanoparticles:

The TEM images (figure 4.20, 4.22, 4.24, 4.26 and 4.28) obtained for silicon depict the formation of different sized nanoparticles of silicon for the different applied electric fields. We varied the electric fields over the range of 0 – 9 V/cm. Experimentally, we found that the size of nanoparticles decreases with increasing electric field as shown in figure 4.30. The experimental parameters and results of the laser ablation of silicon in water are summarized in table 3.

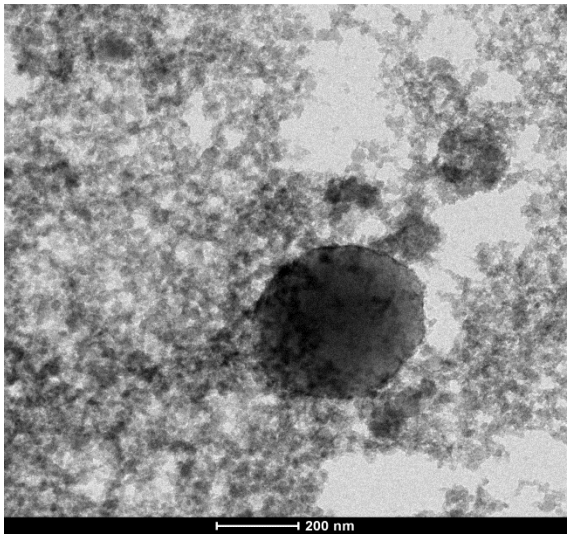

Figure 4.20: TEM image of intermediate nanoparticles of silicon ablated in water when electric field was not applied.

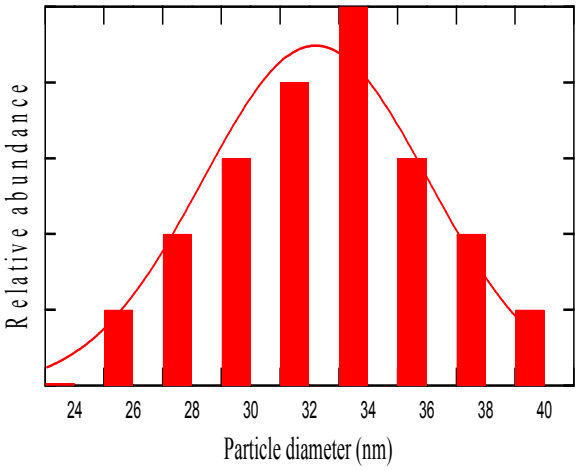

Figure 4.21: Particle distribution of silicon nanoparticles corresponding to Fig.4.20.

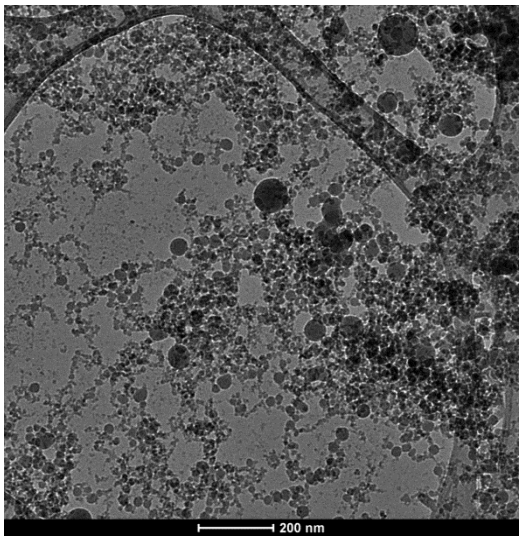

Figure 4.22: TEM image of intermediate nanoparticles of silicon ablated in water at 2.5 V/cm.

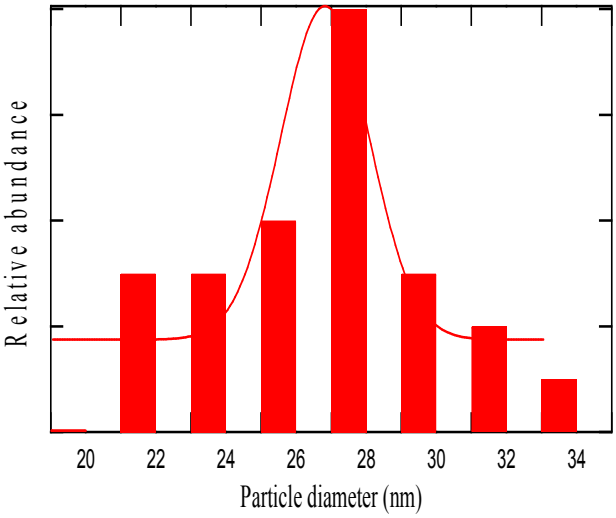

Figure 4.23: Particle distribution of silicon nanoparticles corresponding to Fig. 4.22.

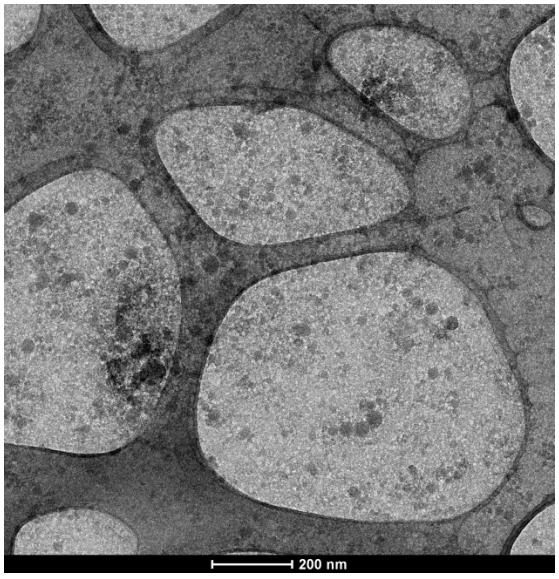

Figure 4.24: TEM image of intermediate nanoparticles of silicon ablated in water at 5 V/cm.

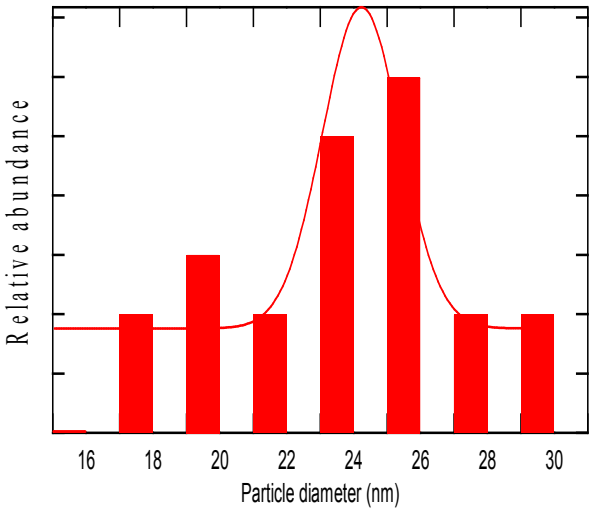

Figure 4.25: Particle distribution of silicon nanoparticles corresponding to Fig. 4.24.

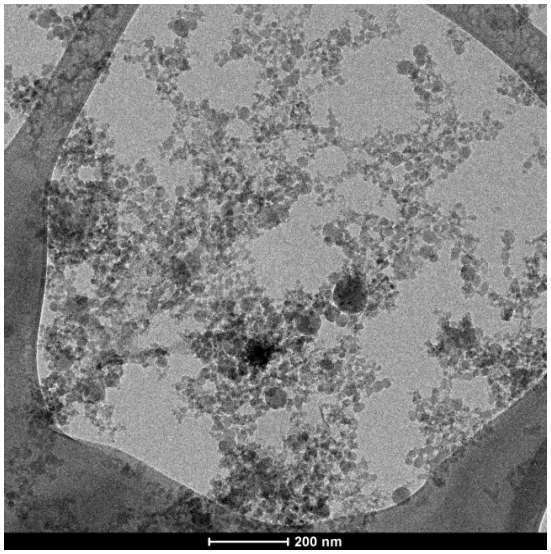

Figure 4.26: TEM image of intermediate nanoparticles of silicon ablated in water at 7.5 V/cm.

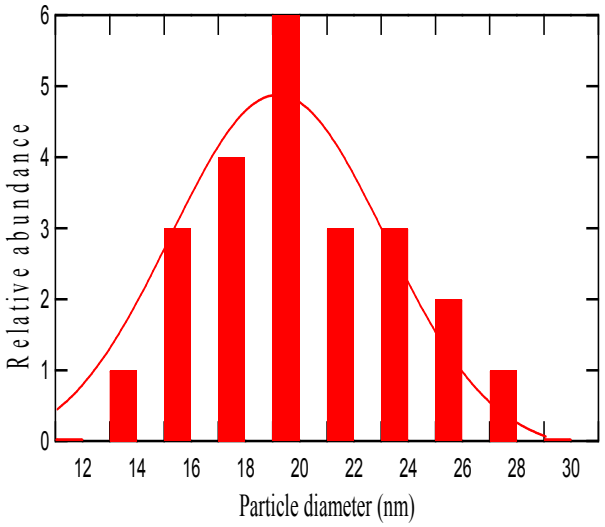

Figure 4.27: Particle distribution of silicon nanoparticles corresponding to Fig.4.26.

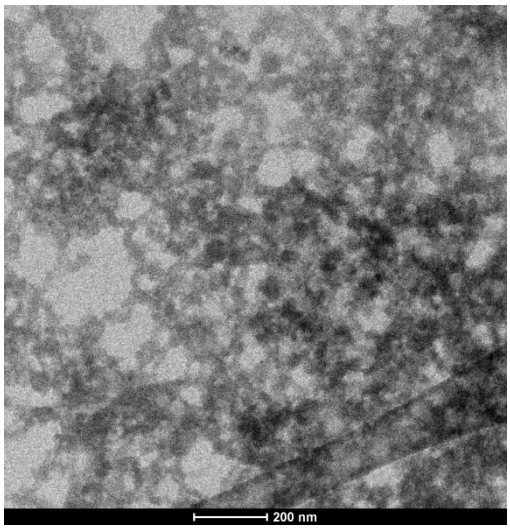

Figure 4.28: TEM image of intermediate nanoparticles of silicon ablated in water at 9 V/cm.

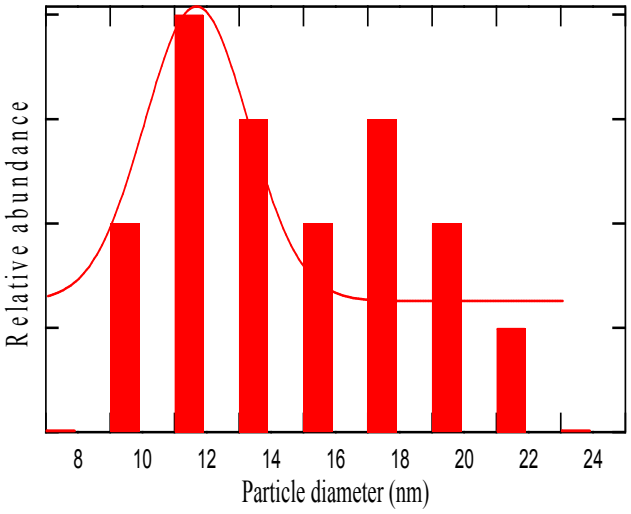

Figure 4.29: Particle distribution of silicon nanoparticles corresponding to Fig.4.28.

Table 3: Summary of experiment of laser irradiation of silicon in water.

S. No.	Electric field (V/cm)	Average size of particles (nm)
1	0	33 ± 5
2	2.5	27 ± 4
3	5	23 ± 3
4	7.5	19 ± 4
5	9	15 ± 4

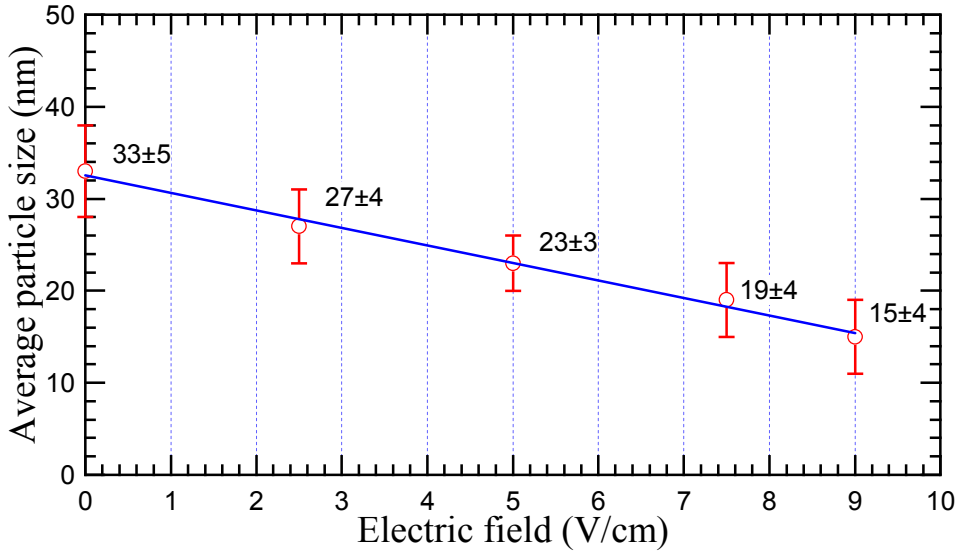

Figure 4.30: Graph of average particle size versus applied voltage for the data collected in table 3 for intermediate nanoparticles of silicon. The blue line is the line of best fit y = a + bx with a = 32.55± 0.57 and b = -1.90±0.09.

We also obtained EDS spectra for the silicon ablation products which confirmed the presence of Si in the colloidal solution prepared by laser irradiation of silicon in water. Figure 4.31 is the EDS spectra showing silicon as well as oxygen, carbon and copper. The silicon peak confirms that the nanoparticles contain silicon.The presence of the oxygen peak may be due to silicon oxide due to the ablation being carried out in distilled water, the oxidized copper from the grid, or both. The peaks due to copper are clearly due to the copper TEM grid.

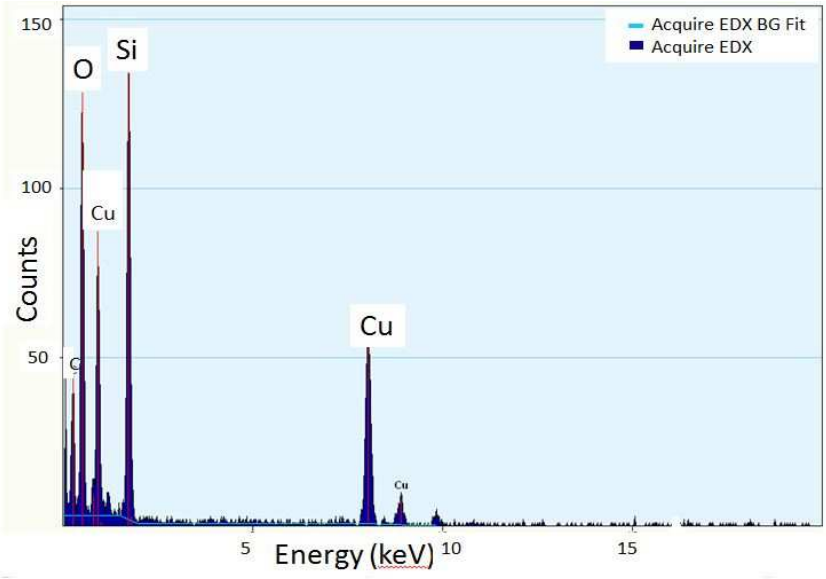

Figure 4.31: EDS spectra of products from silicon ablated in water without an electric field.

4.2 Discussion:

The resulting bimodal size distribution of small and intermediate nanoparticles may be caused by different mechanisms of formation. The formation of nanoparticles is governed by the processes of plasma formation, plume expansion, homogeneous nucleation, and phase explosion. The detail on the formation of nanoparticles had already been discussed in previous section 2.3. Small nanoparticles are formed due to the condensation of atoms of the plume vapor of the ablated material. Intermediate nanoparticles are formed due to the phase explosion in the overheated melt. They may also be formed due to capture of surrounding atoms and electrons in the vapor. In contrast, big sized particles are formed due to hydrodynamic instability, mainly, Rayleigh-Plateau instability.

The applied electric field has a substantial effect on the size of the nanoparticles produced. We observe an influence of the electric field on the nanoparticles, which caused a sharp decrease in size with increase in the magnitude of field. During the process of ablation, due to high fluence, temperature and pressure reach high values. Ionization of the plume takes place. The plume contains electrons, ionized atoms, neutral atoms, clusters and particles with sizes 10 nm or higher. So, the plume is considered as dusty plasma. Because of the high speed of electrons compared to ions, the particles are considered charged (negatively) in the dusty plasma due to capture of the electrons. The charges on the nanoparticles depend on the ionization rate of the plume. In the plume formation, there is a delay between front of the plume formed by mainly electrons and ions and the nanodroplets that are ejected from the surface. An application of electric field makes electrons to move in transversal direction away from the plume. Some electrons will be removed from the plume and will end up in liquid as solvated electrons. This lowers the capture of charges by

nanodroplets. An experiment was performed by Rayleigh[68] on the instability of a charged liquid nanodroplet. According to him, the maximum amount of charge a droplet can carry is given by

$$q_{Rayleigh} = 8\pi(\varepsilon_o \sigma r^3)^{1/2} \qquad (4.1)$$

where q (=ne) is the charge of the droplet, σ is the surface energy per unit area and r is the radius of the droplet. Whenever the charge on the droplet exceeds the critical charge $q_{Rayleigh}$, the droplet becomes unstable and breaks into small droplets. Increase in the externally applied electric field during ablation can assist in increasing the average charges on the particles and results in the fragmentation of the particles in to small particles.

CHAPTER 5

CONCLUSION

5.1 Conclusion:

The irradiation of tin and silicon in distilled water can lead to the removal of material from the solid surface and the formation of nanoparticles. We ablated silicon and tin in water and studied the TEM images of the ablation products. We applied external electric fields during the ablation process in order to investigate the effect on the sizes and morphology of the nanoparticles produced. We found that there is decrease in particle size with increase in the magnitude of applied field. We also noticed that all the nanoparticles produced were spherical in shape. We did not see the effect of the electric field on the shape of particles.

Appendix A

Properties of Silicon

Physical properties:

Symbol ……..... Si
Atomic number ……..... 14
Atomic weight ……..... 28.086
Density at 300K ……..…….. 2.33 g/cm^3
Family in periodic table ……..…… group 14
Crystal structure ……..... cubic
Lattice constant at 300K ……..…….. 0.54311 nm
Dielectric constant at 300K ……..…… 11.9
Index of refraction ……..... 3.42
Bulk modulus ……. 97.6 GPa
Young's modulus ……... 130-188 GPa
Shear modulus …… 51-80 GPa
Poison's ratio ……. 0.064-0.28

Thermal properties:

Melting point …….. 1410^{0}C
Boiling point ……... 3265^{0}C
Heat capacity at 300K (solid) …… 4.78 cal/mol K
Heat capacity at mp (liquid) …….. 6.755 cal/mol K
Latent heat of fusion …….. 50.21 kJ/mol
Latent heat of vaporization …… 383 kJ/mol
Coeff. of linear expansion at 300K …… 2.6x10^{-6} /K
Thermal conductivity at 300K ……... 149 W/mK

Electrical properties:

Intrinsic resistivity ……..…….. 2.4x10^5 Ωcm
Intrinsic electron drift mobility ……..…... 1500 cm^2/Vs
Intrinsic hole drift mobility ……... 600 cm^2/Vs
Band gap at 298K …… 1.12
Band gap at 0K …… 1.17
Number of intrinsic electron …… 1.22x10^{10} cm^{-3}
Electron thermal velocity …….. 2.3x10^5 m/s
Hole thermal velocity …… 1.65x10^5 m/s
Work function …… 4.15 eV
(Source: http://en.wikipedia.org/wiki/Silicon)

Appendix B

Properties of Tin

Physical properties:

Symbol ……... Sn
Atomic number …….. 50
Atomic weight …… 118.71
Density of white β Sn at 300K …….. 7.365 g/cm^3
Family in periodic table ……. group 14
Crystal structure of white β Sn ……. tetragonal
Crystal structure of gray α Sn ……... cubic
Lattice constant at 300K ……... 583.18 pm
Bulk modulus ……. 58 GPa
Young's modulus …… 50 GPa
Shear modulus …… 18 GPa
Poison's ratio ……..…. 0.36

Thermal properties:

Melting point ……... 231.93^{0}C
Boiling point …… 2602^{0}C
Heat capacity at 300K (solid) ……. 217 J/kg K
Latent heat of fusion …… 7 kJ/mol
Latent heat of vaporization ……. 290 kJ/mol
Coeff. of linear expansion at 300K ……. 2.2x10^{-5} /K
Thermal conductivity at 300K …… 67 W/mK

Electrical and magnetic properties:

Electrical resistivity …….. 1.1x10^{-7} Ωm
Electrical conductivity ……. 9.1x10^6 S/m
Superconducting point …….. 3.72
Magnetic type …….. diamagnetic
Mass magnetic susceptibility ……. -3.1x10^{-9}

(source:1.http://periodictable.com/Elements/050/data.html#Tin.SpecificHeat.note
2.http://en.wikipedia.org/wiki/Tin)

BIBLIOGRAPHY

1 G. Palmer, "Lasers", in *Physics for Game Programmers* (Apress, 2005), pp. 385-402.

2 W. Zinth, A. Laubereau, and W. Kaiser, "The long journey to the laser and its rapid development after 1960," The European Physical Journal H **36** (2), 153-181 (2011).

3 O. Svelto, "Properties of Laser Beams", in *Principles of Lasers* (Springer US, 2010), pp. 475-504.

4 W. Schulz, U. Eppelt, and R. Poprawe, "Review on laser drilling I. Fundamentals, modeling, and simulation," Journal of Laser Applications **25** (1), - (2013).

5 C. A. Puliafito, R. F. Steinert, T. F. Deutsch, F. Hillenkamp, E. J. Dehm, and C. M. Adler, "Excimer laser ablation of the cornea and lens. Experimental studies," Ophthalmology **92** (6), 741-748 (1985).

6 B. Bidanda, P. Bártolo, B. R. Ringeisen, J. A Barron, D. Young, C. M. Othon, Doug Ladoucuer, PeterK Wu, and BarryJ Spargo, "Laser Printing Cells", in *Virtual Prototyping & Bio Manufacturing in Medical Applications* (Springer US, 2008), pp. 207-228.

7 B. R. Ringeisen, B. J. Spargo, P. K. Wu, P. Serra, M. Duocastella, J. M. Fernández-Pradas, and J. L. Morenza, "Laser-Induced Forward Transfer: A Laser-Based Technique for Biomolecules Printing", in *Cell and Organ Printing* (Springer Netherlands, 2010), pp. 53-80.

8 G. D. V. Wiggeren and R. Roy, "Communication with Chaotic Lasers," Science **279** (5354), 1198-1200 (1998).

9 A. J. Gross and T. R. W. Herrmann, "History of lasers," World Journal of Urology **25** (3), 217-220 (2007).

10 M. A. Shampo, R. A. Kyle, and D. P. Steensma, "Nikolay Basov—Nobel Prize for Lasers and Masers," Mayo Clinic Proceedings **87** (1), e3-e3 (2012).

11 M. A. Shampo, R. A. Kyle, and D. P. Steensma, "Aleksandr Prokhorov—Lasers and Masers," Mayo Clinic Proceedings **86** (5), e33-e33 (2011).

12 B. G. Sidharth and C. Townes, "The Creative and Unpredictable Interaction of Science and Technology", in *A Century of Ideas* (Springer Netherlands, 2008), Vol. 149, pp. 123-137.

13 "The Nobel Prize in Physics, 1964". Nobelprize.org. Nobel Media AB 2015," (1964).

14 B. Kröger, "Hermann Haken and the “Stuttgart School” 1960 - 1970: Their Contribution to the Development of Laser Theory", in *Hermann Haken: From the Laser to Synergetics* (Springer International Publishing, 2015), pp. 47-99.

15 D. Basting, G. Marowsky, D. Basting, N. Djeu, and K. Jain, "Historical Review of Excimer Laser Development", in *Excimer Laser Technology* (Springer Berlin Heidelberg, 2005), pp. 8-21.

16 M. D. Prasad, "Niels Bohr and the atomic structure," Resonance **18** (10), 897-904 (2013).

17 S. E. Black, *Laser ablation: effects and applications*. (Nova Science Publishers, Hauppauge, N.Y, 2011).

18 M. Paradise and T. Goswami, "Carbon nanotubes – Production and industrial applications," Materials & Design **28** (5), 1477-1489 (2007).

19 S. A. Boppart, J. Herrmann, C. Pitris, D. L. Stamper, M. E. Brezinski, and J. G. Fujimoto, "High-Resolution Optical Coherence Tomography-Guided Laser Ablation of Surgical Tissue," Journal of Surgical Research **82** (2), 275-284 (1999).

20 G. Kamlage, T. Bauer, A. Ostendorf, and B. N. Chichkov, "Deep drilling of metals by femtosecond laser pulses," Applied Physics A **77** (2), 307-310 (2003).

21 S. Bruneau, J. Hermann, G. Dumitru, M. Sentis, and E. Axente, "Ultra-fast laser ablation applied to deep-drilling of metals," Applied Surface Science **248** (1–4), 299-303 (2005).

22 H. M. Smith and A. F. Turner, "Vacuum Deposited Thin Films Using a Ruby Laser," Applied Optics **4** (1), 147-148 (1965).

23 J. Mazumder, O. Conde, R. Villar, W. Steen, and W. W. Duley, "Thin Film Deposition by Laser Ablation", in *Laser Processing: Surface Treatment and Film Deposition* (Springer Netherlands, 1996), Vol. 307, pp. 739-750.

24 C.N.R. Rao, P. J. Thomas, G. U. Kulkarni,"Synthesis of Nanocrystals", in *Nanocrystals: Synthesis, Properties and Applications* (Springer Berlin Heidelberg, 2007), Vol. 95, pp. 25-68.

25 T. Guo, P. Nikolaev, A. G. Rinzler, D. Tomanek, D. T. Colbert, and R. E. Smalley, "Self-Assembly of Tubular Fullerenes," The Journal of Physical Chemistry **99** (27), 10694-10697 (1995).

26 S. Leydecker,"What is nanotechnology?", in *Nano Materials* (B. Basel, 2008), pp. 12-19.

27 D. Bäuerle, "Nanosecond-Laser Ablation", in *Laser Processing and Chemistry* (Springer Berlin Heidelberg, 2000), pp. 221-257.

28 B. N. Chichkov, C. Momma, S. Nolte, F. V Alvensleben, and A. Tünnermann, "Femtosecond, picosecond and nanosecond laser ablation of solids," Applied Physics A **63** (2), 109-115 (1996).

29 P. Patil, D.M. Phase, S. A. Kulkarni, S. V. Ghaisas, S. K. Kulkarni, S. M. Kanetkar, S. B. Ogale, and V. G. Bhide, "Pulsed-laser-induced reactive quenching at liquid-solid interface: Aqueous oxidation of iron," Physical Review Letters **58** (3), 238-241 (1987).

30 G. W. Yang, "Laser ablation in liquids: Applications in the synthesis of nanocrystals," Progress in Materials Science **52** (4), 648-698 (2007).

31 A. V. Simakin, V. V. Voronov, N. A. Kirichenko, and G. A. Shafeev, "Nanoparticles produced by laser ablation of solids in liquid environment," Applied Physics A **79** (4-6), 1127-1132 (2004).

32 N. V. Tarasenko and A. V. Butsen, "Laser synthesis and modification of composite nanoparticles in liquids," Quantum Electronics **40** (11), 986 (2010).

33 C. Phipps, J. Schou, S. Amoruso, and J. G. Lunney, "Plume Dynamics", in *Laser Ablation and its Applications* (Springer US, 2007), Vol. 129, pp. 67-95.

34 X. Mao, W. T. Chan, M. Caetano, M. A. Shannon, and R. E. Russo, "Preferential vaporization and plasma shielding during nano-second laser ablation," Applied Surface Science **96–98** (0), 126-130 (1996).

35 D. Devaux, R. Fabbro, L. Tollier, and E. Bartnicki, "Generation of shock waves by laser-induced plasma in confined geometry," Journal of Applied Physics **74** (4), 2268-2273 (1993).

36 P. Peyre, R. Fabbro, L. Berthe, and C. Dubouchet, "Laser shock processing of materials, physical processes involved and examples of applications," Journal of Laser Applications **8** (3), 135-141 (1996).

37 Y. Jiang, P. Liu, Y. Liang, H. B. Li, and G. W. Yang, "Promoting the yield of nanoparticles from laser ablation in liquid," Applied Physics A **105** (4), 903-907 (2011).

38 C. Nayral, E. Viala, V. Collière, P. Fau, F. Senocq, A. Maisonnat, and B. Chaudret, "Synthesis and use of a novel SnO2 nanomaterial for gas sensing," Applied Surface Science **164** (1–4), 219-226 (2000).

39 C. J. Barbé, F. Arendse, P. Comte, M. Jirousek, F. Lenzmann, V. Shklover, and M. Grätzel, "Nanocrystalline Titanium Oxide Electrodes for Photovoltaic Applications," Journal of the American Ceramic Society **80** (12), 3157-3171 (1997).

40 A. B. Djurišić, A. M. C. Ng, and X. Y. Chen, "ZnO nanostructures for optoelectronics: Material properties and device applications," Progress in Quantum Electronics **34** (4), 191-259 (2010).

41 D. P. L. Zhang, C. M. J. Hu and C. M. Huang, "Development of Nanoparticles for Antimicrobial Drug Delivery", (Bentham Science Publishers Ltd., 2010), Vol. 17, pp. 585-594.

42 F. E. Kruis, H. Fissan, and A. Peled, "Synthesis of nanoparticles in the gas phase for electronic, optical and magnetic applications—a review," Journal of Aerosol Science **29** (5–6), 511-535 (1998).

43 Z. Li, J. C. Barnes, A. Bosoy, J. F. Stoddart, and J. I. Zink, "Mesoporous silica nanoparticles in biomedical applications," Chemical Society Reviews **41** (7), 2590-2605 (2012).

44 J. Salonen, A. M. Kaukonen, J. Hirvonen, and V.P. Lehto, "Mesoporous silicon in drug delivery applications," Journal of Pharmaceutical Sciences **97** (2), 632-653 (2008).

45 G. Ledoux, O. Guillois, D. Porterat, C. Reynaud, F. Huisken, B. Kohn, and V. Paillard, "Photoluminescence properties of silicon nanocrystals as a function of their size," Physical Review B **62** (23), 15942-15951 (2000).

46 L. Tsakalakos, "Nanostructures for photovoltaics," Materials Science and Engineering: R: Reports **62** (6), 175-189 (2008).

47 J. Rong, X. Fang, M. Ge, H. Chen, J. Xu, and C. Zhou, "Coaxial Si/anodic titanium oxide/Si nanotube arrays for lithium-ion battery anodes," Nano Research **6** (3), 182-190 (2013).

48 M. A. F. S. Ahmad, M. Khan , M. K. Rahman and M. A. Tahir, "Synthesis of Iron Oxide–Tin Oxide Nanoparticles and Evaluation of their Activities against Different Bacterial Strains", (Borderless Science Publishing, 2014), Vol. 2, pp. 122-133.

49 W. Göpel, "Ultimate limits in the miniaturization of chemical sensors," Sensors and Actuators A: Physical **56** (1–2), 83-102 (1996).

50 G. Cui, Y. S. Hu, L. Zhi, D. Wu, I. Lieberwirth, J. Maier, and K. Müllen, "A One-Step Approach Towards Carbon-Encapsulated Hollow Tin Nanoparticles and Their Application in Lithium Batteries," Small **3** (12), 2066-2069 (2007).

51 A. A. Serkov, E. V. Barmina, G. A. Shafeev, and V. V. Voronov, "Laser ablation of Titanium in liquid in external electric field," Applied Surface Science (0) (2014).

52 R. A. Ismail and F. A. Fadhil, "Effect of electric field on the properties of bismuth oxide nanoparticles prepared by laser ablation in water," Journal of Materials Science: Materials in Electronics **25** (3), 1435-1440 (2014).

53 M. A. Ordal, L. L. Long, R. J. Bell, S. E. Bell, R. R. Bell, R. W. Alexander, and C. A. Ward, "Optical properties of the metals Al, Co, Cu, Au, Fe, Pb, Ni, Pd, Pt, Ag, Ti, and W in the infrared and far infrared," Applied Optics **22** (7), 1099-1119 (1983).

54 D. W. Lynch, W. R. Hunter, and D. F. Edwards, "Handbook of optical constants of solids", edited by E.D. Palik (Academic Press, 1998), pp. 268,356.

55 R. B. Tagirov and L. P. Tagirov, "Lambert formula — Bouguer absorption law?," Russian Physics Journal **40** (7), 664-669 (1997).

56 M. M. A. G. Jafar, "Comprehensive formulations forthe total normal-incidence optical reflectance andtransmittance of thin films laid on thick substrates", (European International Journal of Science and Technology, 2013), Vol. 2, pp. 214-274.

57 R. F. Wood and G. E. Giles, "Macroscopic theory of pulsed-laser annealing. I. Thermal transport and melting," Physical Review B **23** (6), 2923-2942 (1981).

58 R. K. Singh and J. Narayan, "A novel method for simulating laser-solid interactions in semiconductors and layered structures," Materials Science and Engineering: B **3** (3), 217-230 (1989).

59 A. D. Boardman, B. Cresswell, and J. Anderson, "An analytical model for the laser ablation of materials," Applied Surface Science **96–98** (0), 55-60 (1996).

60 S. Amoruso, R. Bruzzese, R. Velotta, N. Spinelli, and X. Wang, "Characterization of laser-ablation plasmas", (Journal of Physics B, 1999), Vol. 32, pp. 131-172.

61 D. A. Willis and X. Xu, "Heat transfer and phase change during picosecond laser ablation of nickel," International Journal of Heat and Mass Transfer **45** (19), 3911-3918 (2002).

62 N. M. Bulgakova, A. V. Bulgakov, and L. P. Babich, "Energy balance of pulsed laser ablation: thermal model revised," Applied Physics A **79** (4-6), 1323-1326 (2004).

63 A. M. Prokhorov, V. I. Konov, I. Ursu, and N. Mihailescu, "Laser Heating of Metals", (CRC Press, 1990).

64 X. Xu, "Non-Equilibrium Phase Change in Metal Induced by Nanosecond Pulsed Laser Irriadiation", edited by David A Willis (Journal of Heat Transfer, 2002), Vol. 124, pp. 293-298.

65 D. W. Blair, S. S. Harilal and M. S. Tillack, "The effect of ionization on cluster formation in laser ablation plumes", (Institute of Physics Publishing, 2004), Vol. 15, pp. 390-403.

66 J. K. C. Unger, L. Overmeyer and B. N. Chichkov, "Time-resolved studies of femtosecond-laser induced melt dynamics," **20** (22), 24864-24872 (2012).

67 O. R. Musaev, J. Yan, V. Dusevich, J. M. Wrobel, and M. B. Kruger, "Ni nanoparticles fabricated by laser ablation in water," Applied Physics A **116** (2), 735-739 (2014).

68 C. S. Fong, N. D. Black, P. A. Kiefer, and R. A. Shaw, "An experiment on the Rayleigh instability of charged liquid drops," American Journal of Physics **75** (6), 499-503 (2007).

VITA

Deepak Sapkota was born on June 24, 1982 in Syangja, Nepal. He completed his high school from a local school in 2001. He joined Birendra Multiple Campus and he graduated in B.Sc. in Physics in 2004 from there. In 2006, he completed his M.Sc. in Physics and he was awarded this degree from Tribhuvan University.

He started teaching Physics to high school students when he was pursuing his Baccalaureate degree in 2001. After finishing his MS degree in 2006, he joined a college as physics lecturer. He taught physics to high school students and to undergraduate students for five years in different institutions.

To further his study of physics, he applied to and was admitted to the University of Missouri-Kansas City. He served as GTA in the Department of Physics and Astronomy for two years. Meanwhile, he joined a research group working on experimental condensed matter physics under the supervision of Prof. Michael Kruger. He focused his research study on the laser ablation of different elements and the effect of externally applied electric field on the different physical parameters of nanoparticles formed during the process of irradiation. Upon completion of his Master's degree, he plans to continue his research study in physics by joining a Ph.D. program.